Quantized Constant-Q Gabor Atoms for Sparse Binary Representations of Cyber-Physical Signatures

Milton A. Garces[1,2]*

[1] Infrasound Laboratory, University of Hawaii, Manoa; milton@isla.hawaii.edu
[2] RedVox, Inc.; milton@redvoxsound.com
* Correspondence: milton@isla.hawaii.edu

Abstract: Increased data acquisition by uncalibrated, heterogeneous digital sensor systems such as smartphones present new challenges. Binary metrics are proposed for the quantification of cyber-physical signal characteristics and features, and a standardized constant-Q variation of the Gabor atom is developed for use with wavelet transforms. Two different CWT reconstruction formulas are presented and tested under different SNR conditions. A sparse superposition of Nth order Gabor atoms worked well against a blast synthetic using the wavelet entropy and an entropy-like parametrization of the SNR as the CWT coefficient-weighting functions. The proposed methods should be well suited for sparse feature extraction and dictionary-based machine learning.

Keywords: Gabor atoms; wavelet entropy; binary metrics; acoustics; quantum wavelet

1. Overture

This paper applies the constant-Q standardized Inferno framework of Garces (2013) to the Gabor wavelet and proposes binary metrics for signature characterization. I assume a cyber-physical sensor system converts observables into digital time series data consisting of a combination of signals and noise. A signal of interest can be hypothetically described by sparse representations that define its signature. If its signature characteristics are sufficiently unique and recognizable from those of ambient coherent and incoherent noise, it can be used to identify and classify an object or process.

The transformation of diverse digital measurements into robust, scalable, and transportable representations is a prerequisite for signal detection, source localization, and machine learning applications for signature classification. The challenge at hand is to construct sparse signal representations that contain sufficient information for classification. Unambiguous classification can be elusive; measurement artifacts, unexpected signal variability, and non-stationary noise often conspire to add uncertainty to our classifiers. As will be discussed in this paper, information and uncertainty quantification can be substantially simplified when using standardized wavelets and binary metrics.

2. About Time

Oscillatory processes often exhibit spatial and temporal scalability and self-similarity. Although some physical processes scale linearly, many exhibit recurrent patterns that scale logarithmically and are well represented by power laws. Both linear and logarithmic scales can coexist. For example, overtones in harmonic acoustic systems are often linearly spaced in frequency, yet our sense of tone similarity is close to base 2 logarithmic (binary) octave scales. The term octave comes from the eight major notes in 12-tone musical notation, which closely repeat in with factors of two. In this paper I will use the term

octave and binary interchangeably to denote the base 2 geometric scaling of frequency and time. The mapping between frequency (or pitch) and time (period) is direct for continuous tones, such as musical notes, or statistically stationary oscillations like the orbits of planets. Discrete Fourier transform methods are exceptionally well suited for the interpretation of steady tonal signals with linearly spaced harmonics. The Fourier transform deconstructs oscillations with distinct recurrent time periods into a *spectral* representation consisting of a set of discrete frequencies. The spectral transformation can be sparse because it removes time as a variable, making it possible to readily reconstruct stable oscillations from a subset of coefficients in the Fourier spectrum.

Stable oscillators can be even more succinctly represented by a fundamental frequency *or* period (exclusive *or,* they are not independent). For many physical systems, a map can be constructed between the fundamental and its harmonics. Signals where the fundamental and its harmonics (when they exist) are statistically stationary and easily discernible above noise are referred to as the easy *continuous wave* (CW) problem, or the zeroth (trivial) class of CW problems. The trivial CW problem is well understood and should routinely be used as a speed and performance benchmark for detection and classification algorithms.

The plot thickens when temporal variability is introduced in signal or noise. In the first class of CW problems, temporal variability is due to increased broadband or band-limited noise. This is an exceptionally valuable sensitivity exercise for array processing, where noise can be coherent or incoherent across the array aperture. The first class of CW problems is also well understood when noise is normally distributed over a time duration that is a substantial multiple of the signal period in the detection band. However, this class of problems is not as well characterized when noise is not evenly distributed across the signal detection bandpass, and can be particularly inconvenient when noise steps on the fundamental frequency.

In the second class of CW problems, temporal variability is introduced by a change in the temporal, spectral, and/or statistical properties of the signal. These changes can be due to aging, failure, motion, communication, or any other change in state. In a simple two-state problem, one may quantify the properties of the first state, the transition period between states, and the properties on the final state. In a multiple-state problem, such as with communication systems, speech, or music, the short-term discrete Fourier transform (STFT) is often used to characterize spectral variability. This can be a complicated class of problems in the presence of noise.

If the transition period between states is faster that the characteristic time scale of the initial state, the STFT does not always provide an accurate representation of this *transient*. For some signals, the details of the transient are not relevant and only the steady states are important. But a new class of signals emerges when the detection of transient anomalies is prioritized.

The zeroth class of transient problems consist of delta functions with their integrals and derivatives: instantaneous spikes which do not exist in the natural world but can be readily constructed digitally and routinely used in the evaluation of the impulse response of a system. The first class of transient problems would be more realistic variants of the delta function that may be observed in the wild when a rapid change of state becomes the signal of interest. Just like a single-tone sinusoid may be regarded as the prototype end member for the trivial CW problem, an explosive detonation could be considered as a prototype transient signal source. During an explosion, observations would vary from ambient noise to a brief blast transient that fades back to a possibly perturbed ambient noise state. If the observations were acoustic at some distance from the source, the system would go from quiescence to blast to quiescence, and the transition can be devastatingly fast. In general, poorly-conditioned STFTs provides inadequate representations of brief, rapidly changing signals because the signatures no longer resemble a CW, and so are not well represented by sinusoids. However, since a STFT is a windowed sinusoid, a well-conditioned STFT window at the peak frequency of a signal turns the waveform into a wavelet.

The concept of a windowed sinusoid to represent a transient signal was introduced by Gabor (1946), and later mathematically formalized by others as wavelets. Variants of the Gabor wavelet are presented in the Appendices.

The second class of transient problems overlaps with the second class of CW problems. It corresponds to transients of significant durations which could be addressed with STFTs, wavelets, or their combination. Very often a transient is imbedded in a noise field with band-limited harmonic structure. Or the transient itself is a sweep, characterized by a substantial frequency change in the fundamental and its harmonic structure.

The primary differences between STFTs and wavelet approaches are that the former uses a linear period mapping and a constant processing window duration and the latter uses geometric pseudo-period mapping and a window duration that scales with the pseudo-period. Whereas in the Fourier framework there is a one-to-one mapping between time and frequency, the wavelet mapping between time scale and frequency can be less evident and depends on the selected wavelet.

In this paper I concentrate on developing standardized constant-Q Gabor atoms for the design and evaluation of transportable, sensor-agnostic signal detection, sparse feature extraction, and classification algorithms.

3. Quantifying Information in Cyber-Physical Systems

Cyber-physical systems (CPS) are algorithm-controlled computer systems with physical inputs and outputs. A typical example of a mobile CPS is a smartphone with a microphone input (sound activation) that outputs a response (speech, music, or signal recognition) to a screen. Cyber-physical Measurement and Signature Intelligence (MASINT) was defined by Pecenak et. al. (2018) and Cai et al. (2019) as an emerging branch that concentrates on phenomena transmitted through cyber-physical devices and their interconnected data networks. For smartphones and other multi-sensor mobile platforms connected to wireless networks, this must include digital noise, bit errors, and latencies internal to the device and its communication channels.

Data processed by the cyber part of CPSs are digital and represented as binary digits (bits). Although the precision of the data is initially defined by its their integer symbol length (16, 32, 64 bit, etc.), the data may convert into float equivalents when an algorithms acts on it. For example, consider sound recorded by a smartphone at the standard rate of 48,000 samples per second. A typical sound record may have 16-bit resolution, so that its dynamic range in bits is 2^{-15} to $2^{15} - 1$. However, one may only be interested in the lower frequency components of the raw data, so one would implement a lowpass anti-aliasing before decimation. Such filters require double precision (64 bit at the time of this writing) to reduce instability. Therefore the precision of the resulting lowpass filtered data would be float 64. However, the theoretical dynamic range of the system would not exceed the specification of the integer 16 physical input. Furthermore, data compression can be more efficient on floats than integers, which leads us to the topic of fractional bits as a measure of CPS amplitude, power, and information.

Many of the metrics we used in traditional physical and geophysical systems are inherited from the analog era. The base 10 decibel scale is a measure of power relative to a reference level, and is used extensively in telecommunications, acoustics, and electrical engineering. Let's estimate the hypothetical dynamic range of a 16-bit microphone record of a sinusoid at full scale. The peak rms amplitude would be

$$p_{rms\ signal} = \frac{2^{16}}{2\sqrt{2}}$$

All systems have quantization and system noise, and it can have a positive or negative bias. This is not a noise paper; for the sake of illustration, I model the system noise as oscillating around a mean of zero and alternating between -1 and 1,

$$p_{rms\ noise} = \frac{2^1}{2\sqrt{2}}$$

The theoretical dynamic range of the system in dB for a sinusoid recorded with a 16-bit microphone and sound card combination with a one-bit noise floor could be characterized by the ratio of the power

$$10 * log_{10} \left[\frac{p_{rms\ signal}}{p_{rms\ noise}} \right]^2 = 20 * log_{10}[2^{15}] \approx 90 dB$$

Where we have converted a digital response to the legacy base 10 logarithmic system. One advantage of the decibel approach is that it can be compared to the response of the human ear and other analog systems. However, analogue comparisons are not necessary for many cyber physical applications. A more natural unit for CPS is the binary logarithm

$$log_2 \left[\frac{p_{rms\ signal}}{p_{rms\ noise}} \right] = log_2[2^{15}] \approx 15.0\ fbits$$

Where the unit *fbits* corresponds to floating point representation of bits. For example, in 24-bit systems, present-day quantization error is ~3 bits, leading to an effective dynamic range of ~21 fbits. Likewise, a 24-bit integer cast into a 32-bit symbol can have 8+3 bits of noise, and may be converted to a float that still has ~21 fbits of dynamic range.

Another unit that is often specified is the ½ power point of the frequency response of a filter, which defines the quality factor of that filter. This is often referred to as the -3dB point, since $10 * log_{10}(2) \sim 3dB$. However, accurate filter bank reproductions require a clear specification of the ½ power point, and conversion from base 10 to base 2 specification can lead to computational errors. Plotting filter responses in floating point bits can be informative as it reveals the precision of the computation. Because it is awkward and there is already a precedent in information theory for using bits outside of their original definition as a binary digit, from here onwards in this paper the word bits will be used to represent either the floating point equivalent of bits or as a metric for information.

Consider the communication channel capacity introduced by Shannon [1949], which in its simplest form can be expressed as

$$Ch = W log_2 \left(\frac{Sg + Ns}{Ns} \right)$$

where Ch is a measure of the differential entropy of a signal in the presence of noise, W is a measure of the bandwidth, Sg is representative of the power of a signal, and *Ns* is representative of the noise power. The units of the channel capacity are in shannons, or bits per second, and represents the theoretical upper bound of the rate of information transfer in a communication channel. Since it is often impossible to separate noise already in a signal but it is often possible to construct a noise model, we can think the ratio *(Sg+Ns)/Ns* as a practical measure of the signal to noise ratio (SNR) of an observed signal that has been carried through a processing system or a medium.

The effective SNR and therefore the detectability of a compressed pulse (such as a wavelet) is the product of the bandwidth, the signal to noise ratio, and the duration of a signal T. When using constant-Q Gabor wavelet with fractional octave (binary) bands n of order N and center frequency f_n to process a signal in the presence of noise, I show that for

$$SNR_n = \frac{Ns_n + Sg_n}{Ns_n} = 1 + \frac{Sg_n}{Ns_n}$$

the signal detectability per band can be represented by

$$bSNR_n = \frac{1}{2} \, log_2(SNR_n) \ .$$

And the upper limit on rate of information in bits per second for a band-limited pulse with center frequency f_n can be estimated from

$$Ch_n = \frac{f_n}{N} \, bSNR_n$$

Energy and Shannon entropies using the binary log are constructed for both the wavelet coefficients and SNR in a later section.

4. Binary Quantized Constant-Q Gabor Atoms

Gabor (1946) extended the Heisenberg principle to define the time-frequency uncertainty principle, and further proposed deconstructing signals into elementary waveforms he referred to as time-frequency atoms (e.g. M09) that provide the optimum compromise between time and frequency resolution and thus maximize information density. Its functional kin, the Morlet wavelet, was developed for seismic applications and is much beloved by mathematicians. Much has been said and written over the last 75 years about the merits, and limitations (e.g. Sheu et al. 2014), of the Gabor atom in diverse fields of applied science ranging from quantum mechanics (e.g. Ashmead 2012), neurophysiology (e.g. Canolty and Womelsdorf, 2019), and radar target recognition (Shi and Zhang, 2001). Additional details and references are provided in the Appendixes.

The Gabor wavelet atom is a translation and dilation of its familiar mother wavelet

$$\Psi(x) = \frac{1}{\pi^{1/4}} exp\left(-\frac{x^2}{2}\right) exp\left(i\Omega_N x\right)$$

with dictionary (M9)

$$\Psi_{\eta',n}(\eta) = \frac{1}{\sqrt{s_n}} \Psi\left(\frac{x-x'}{s_n}\right)$$

$$\Psi_{x',n}(t) = \frac{1}{\pi^{1/4}} \frac{1}{\sqrt{s_n}} exp\left\{-\frac{1}{2}\left[\frac{x-x'}{s_n}\right]^2\right\} exp\left\{i\Omega_N\left[\frac{x-x'}{s_n}\right]\right\}$$

The constant-q Gabor atoms are constrained to the range of values

$$s_n = s_0 2^{\frac{n}{N}} = \frac{\Omega_N}{2\pi} f_s \tau_n, \quad \Omega_N = 2\sqrt{ln2} \, Q_N$$

with quality factor

$$Q_N = \left[2^{\frac{1}{2N}} - 2^{-\frac{1}{2N}}\right]^{-1}$$

defined by the ½ power points of the Fourier spectrum. Details of the derivations are provided in Appendices A-C. For this functional form, the wavelet admissibility condition can be represented as

$$\Omega_N^2 \gg 1$$

Although in principle $n \in \mathbb{Z}$, $N \in \mathbb{R} > 0$, for a given bandpass of interest the recommended quanta for the Gabor atoms are positive integer band numbers n and the preferred orders N as in Garces (2013),

$$n = 0, 1, 2 \dots, \quad N = 1, 3, 6, 12, 24 \dots$$

though the special orders N=0.75 and 1.5 will be considered. The mother wavelet is uniquely defined (and can be quantized) by the order N, although it is often specified by the more accessible variable Ω_N. The mother wavelet is scale invariant. Each discrete atom in its dictionary is defined by its order N, its band number n, and a refence scale at n=0. If the Gabor atoms remain within their quanta, there is only one degree of freedom: the reference scale. The reference scale can be set by the data acquisition system (e.g. the Nyquist frequency) or a standard frequency (for example, 1kHz in acoustic applications, 1Hz in infrasound applications). It can also be set by a signal tuning frequency; the peak frequency for a detonation is used in Section 7. When integrating multi-sensor time series with different evenly and unevenly sampled data, it is better to either use a standard reference frequency or time scale (e.g. 1 kHz, 1 s, 1 hour) or the target frequency. The resulting bands will be evenly spaced to standardize and facilitate multi-sensor cross-correlations and data fusion. However, it is important to recognize that the mapping from nondimensional scale to physical time scale depends on the sample rate. Inversely, specifying a sample rate f_s or a sample interval $\Delta\tau_s = 1/f_s$ permits conversion to physical time t and time scales τ_n in units of the sample interval,

$$t = \frac{x}{f_s}, \qquad s_n = \frac{\Omega_N}{2\pi} f_s \tau_n, \qquad \tau_n = \tau_0 2^{\frac{n}{N}}$$

and correspond to the peaks in the Fourier spectrum at the frequencies,

$$f_n = f_0 2^{-\frac{n}{N}} = \frac{1}{\tau_n}, \qquad \omega_n = 2\pi f_n$$

It may be useful to think of the binary (base 2) order N as the quantized time and bandwidth stretch factor of the Gabor atom; as the order increases, the wavelet stretches in time and narrows in bandwidth, with each frequency band occupying a constant proportional frequency bandwidth that produces Q_N oscillations at the band frequency in the time domain. As noted a few sentences up in sparser mathematical notation, although in theory it is possible to use any integer band indexes n, the recommended best practice is to use only nonnegative integers to represent temporal scales, with τ_0 corresponding to the smallest scale and ω_0 to the highest frequency below the Nyquist frequency.

The Gabor wavelet and its Morlet kin are attractive to engineers, physicists and mathematicians as they combine two beloved oscillatory and decay functions. They are also popular in information theory as a Gaussian-wrapped oscillation in general, and the Gabor atom in particular, meet the minimal value for the Heisenberg-Gabor uncertainty principle, where the temporal variance σ_t^2 and angular frequency variance σ_ω^2 over all time and frequency satisfy

$$\sigma_t \sigma_\omega = \frac{1}{2}$$

This wavelet can be quantized using the well-known fixed order N and quality factor Q_N values of standard geometric binary intervals referred to as fractional octave bands in acoustic and infrasound applications (Table 1).

Table 1. Quality factor Q and Ω for standard fractional octave bands of order N [1].

N	Q_N	Ω_N
1	1.4142	2.3548
3	4.3185	7.1907
6	8.6514	14.4055
12	17.3099	28.8229
24	34.6235	57.6519
48	69.2488	115.3067
96	138.4984	230.6150

[1] Dyadic base, G=2.

Appendix A develops a useful approximation for the quality factor Q_N of order N,

$$Q_N \approx \sqrt{2}N \approx 1.414\,N, \quad M_N = 2\sqrt{ln2}\,Q_N \approx 2\sqrt{2ln2}\,N \approx 2.355\,N$$

with exact equivalence for octave bands at N=1 (Table 2).

Table 2. Exact and approximate quality factor Q for standard fractional octave bands of order N [1].

N	Q_N	$Q_N \approx \sqrt{2}N$
1	1.4142	1.4142
3	4.3185	4.2426
6	8.6514	8.4853
12	17.3099	16.9706
24	34.6235	33.9411
48	69.2488	67.8823
96	138.4984	135.7645

[1] Dyadic base, G=2.

These relations are seldom made explicit for constant Q wavelet representations, which often leads to inadvertently creative interpretations and implementations. In traditional fractional octave bands, N is an integer with preferred numbers 1, 3, 6, 12, 24 and its half-power (-3 dB) band edges and center frequencies are well established so their Q can be readily computed (Tables 1 and 2). The band spectrum will overlap at the half-power point band edges to reduce (or at least regulate) spectral leakage and improve energy estimation. Dyadic wavelets use order N=1 and are weakly admissible ($\Omega_N^2 \sim 5.54$); carefully handled they do lead to very sparse and fast computational implementations (e.g. M9).

The estimate for Q_N in terms of the order N is useful for practical application where we wish to specify the number of oscillations Q_N in a window. If one abandons the bounds of the preferred bands, one can estimate the order for a wavelet that has any number of oscillations in its support window. Once N is estimated, exact values for the center frequencies and band edges can be computed from the expressions in Appendix A. These bespoke constant-Q bands will not meet binary (factor of two) recursions with ½ power bandedge overlap, but may be useful for highly customized tuning. Examples are provided in Table 3.

Table 3. Approximate quality factor Q and Ω for non-integer order N [1].

Q_N	$N \approx Q_N/\sqrt{2}$	Ω_N
1	0.7071	1.6651
2	1.4142	3.3302
4	2.8284	6.6604
8	5.6569	13.3209
16	11.3137	26.6417
32	22.6274	53.2835
64	45.2548	106.5670
128	90.5097	213.1340

[1] Dyadic base, G=2.

Consider the curious case of a single oscillation in the window, where

$$N = \frac{3}{4} = 0.75, \qquad Q_N = 1.04, \qquad \Omega_N = 2\sqrt{ln2} \approx 1.74$$

and Q is evaluated more precisely from the order N. Although intuitive and compact, the resulting wavelets are marginally admissible ($\Omega_N^2 \sim 3$) and produce oddly spaced, but legitimate, constant-Q frequency bands that grow rapidly and hit only every fourth standard octave (power of two) every three bands. The window duration will be only 1.74 periods long and the spectral resolution of the Fourier transform will be exceedingly sparse. Adding another oscillation per window (increasing the quality factor to two), would correspond to

$$N = \frac{3}{2} = 1.5, \qquad Q_N = 2.14, \qquad \Omega_N = 2\sqrt{ln2} \approx 3.57$$

The resulting wavelets that are more admissible ($\Omega_N^2 \sim 12.8$) but also produced oddly spaced constant-Q frequency bands that land on every second standard octave every three bands. Third order bands hit exact powers of two every third band and have around four oscillations per window (Appendix D). Although it is possible to force center frequency scales, if best practices for band overlap are ignored one will have a set of wavelet filter banks with substantial spectral leakage or gaps between adjacent bands, and the possibility for excessively overdetermined or underdetermines results. This is what usually happens with default parameters on most CWT or DWT algorithms. This paper standardizes and regulates band spacing by asserting the relationship between order, bandwidth, and duration. Since it is both silly and mathematically inadvisable (even inadmissible) to construct a wavelet with less than one oscillation in its window, so it is recommended that $Q \geq 1$. This suggests a minimum order number (quantum) of N=3/4 for stable Gabor atoms, with N=1 yielding value exact power of two (binary) bands.

It is possible to estimate the smallest possible universal binary scale from the Planck time, the smallest measurable time scale

$$\Delta\tau_{Planck} = 10^{-43}s \sim 2^{-142}s$$

Since the Planck time would be the smallest possible sample interval, the smallest oscillation that could be observed would be at the universal Nyquist period

$$\tau_{min} = 2\Delta\tau_{Planck} \sim 2^{-141}s$$

At the other end of the timeline, the age of the universe is estimated to be 13.8 billion years, or

$$\tau_{max} \sim 2^{58} \, s$$

So that the (presently) known universe can be encompassed in the range of ~200 temporal octave bands. Computationally speaking, this is a small range of octaves that can be spanned by 200 temporal Gabor atoms. Earth is estimated to be ~4.6 billion years old, covering around about 57 of those temporal binary bands, and the oldest bones associated with Homo Sapiens-Sapiens are ~200,000 years old and within the last 42 temporal sub-bands since Earth's inception. The human voice for average individuals ranges between one and two octaves, and five octaves species-wide. A third order representation (N=3) of all the times scales in the universe can be represented by only 600 temporal Gabor atoms. In principle it would be possible to construct universal scales with $\tau_0 = 2^{-141}s$, whereas all timescales would occupy temporal sub-bands, but it is not clear there would be practical value to it.

The beauty of the third order representation is that it is very close to the decimal representation, with every ten 1/3 octaves producing a decade $(2^{10/3} \sim 10)$, and thus provide a geometrically elegant compromise between ten-digit humans and binary digit machines. In addition to better meeting the admissibility condition, third order bands will contain over 99% of the information within their octave (Appendix E), making them compact temporal carriers. If the third order representation is used as the base order (N=3), the preferred numbers are binary multiples (N = 3, 6, 12, 24 in Table 1), with a proportional elongation in the wavelet support and increase in spectral resolution.

The nondimensionalized binary scale s at the Nyquist frequency is always the same regardless of whether one uses the Plank scale or half the age of the known universe (which would be not only impractical but not very informative as it would only leave one octave to process)

$$Q_1 = \sqrt{2}, \qquad \Omega_1 = 2\sqrt{2ln2}, \qquad s_0 = \frac{\Omega_1}{2\pi}\frac{\tau_{min}}{\Delta\tau_{Planck}} = \sqrt{\frac{ln2}{2\pi^2}}$$

$$s_n = s_0 2^n$$

Many software packages readily produce a Gabor-Morlet wavelet with default parameters. One of the most common values is $\Omega_N = 5$, which is close to order $N = 2$ (Table 4). Other common values of the wavelet support correspond to $\Omega_N = 4$, $N = 1.7$ and the more reasonable $\Omega_N = 8$ which is close to preferred order $N = 3$.

Table 4. Approximate quality factor Q and order N for commonly used values of Ω.

Ω_N	$\sim Q_N$	N
1	0.600561204	0.4246609
2	1.201122409	0.8493218
4	2.402244818	1.698643601
5	3.002806022	2.123304501
6	3.603367226	2.547965401
8	4.804489635	3.397287201

[1] Dyadic base, G=2.

Because none of these specifications correspond to standard orders, the resulting wavelets will tend to either overestimate (due to spectral leakage) or underestimate (due to spectral gaps between bands) the energy within adjacent binary bands when forced, or will produce oddly spaced bands.

Although it is possible to quantize the constant-Q Gabor atoms using the order N, the quality factor Q, or the multiplier Ω, since the lowest recommended order is N=1 it would be more natural to use it to define the quantum order of the wavelet. As the jaded joke goes, naming things is hard. Describing the proposed wavelet dictionaries of preferred orders as the quantized constant-Q Gabor atoms with binary bases and overlapping ½ power points is rather awkward, and this paper I propose referring to these constructs as quantized wavelets, quantum wavelets of order N, or Nth order Gabor atoms. Whether this naming survives the upcoming review process remains to be seen, and the author is open to suggestions. Although N=1 provides the sparsest clean binary (with power of two steps in frequency) representation with the tightest windows, the admissibility condition coupled with the better reconstruction capability presented in the next section suggest that using N=3 as the base order is preferable, with the added advantage that all subsequent preferred orders in Table 1 are binary factors of base order 3.

5. Continuous Wavelet Transform Deconstruction and Reconstruction

The continuous wavelet transform (CWT) of a function $g(t)$ is represented in M9 (Eq. 1.13) as

$$\mathcal{W}(g, u, s) = \langle g, \Psi_{u,n} \rangle = \int_{-\infty}^{\infty} g(t) \frac{1}{\sqrt{s}} \Psi^* \left(\frac{t - u}{s} \right) dt$$

where (*) represents the complex conjugate. The equivalent CWT for a discrete sequence of observations (or a synthetic time series) $g(m)$ is the convolution of g with a scaled and translated version of $\Psi(m)$. Consider the nondimensional Quantum mother wavelet of order N,

$$\Psi_N(m) = \frac{1}{\pi^{1/4}} exp \left(-\frac{m^2}{2} \right) \exp \left(i\Omega_N m \right)$$

$$\Psi_{u,n}(m) = \frac{1}{\sqrt{s_n}} \Psi_N \left(\frac{m - u}{s_n} \right)$$

$$s_n = \frac{\Omega_N}{2\pi} f_s \tau_0 2^{\frac{n}{N}} = s_0 \, 2^{\frac{n}{N}}.$$

After M9, define

$$\Psi_n[m] = \frac{1}{\sqrt{s_n}} \Psi \left(\frac{m}{s_n} \right)$$

The discrete CWT can be expressed as

$$\mathcal{W}_n[m] = \sum_{m'=0}^{Mp-1} g(m') \Psi_n^*(m' - m) = g \circledast \Psi_n^*[m]$$

Where the symbol $\circledast$ denotes a convolution (M9), often computed using the Discrete Fourier transform (Scipy). This is comparable to the expression in Torrence and Compo (1998), although their convolution has no amplitude scaling as it is corrected afterwards. The CWT coefficients $\mathcal{W}_{m,n}$ provide a measure of the degree of similarity between the time series and the wavelet of scale index n while translating along the time index m. While exact waveform reconstruction from the CWT is challenging (e.g. Ferges, 1992; Lebedeva and Postnikov, 2014), Torrence and Compo (1998) provide an approximate expression for the wavelet-filtered time series $g'(m)$. The reconstruction filter from the Nth order Gabor atoms becomes,

$$g[m] \approx \frac{\pi^{\frac{1}{4}}}{N} \frac{1}{C_\delta} \sum_{n=0}^{Np-1} \frac{Re\{\mathcal{W}_n[m]\}}{\sqrt{s_n}}$$

Where Re{ } denotes the real part of the coefficients and the reconstruction factor C_δ is scale independent and constant for wavelet function with fixed M_N. The reconstruction factor can be estimated by comparing against known test functions. Torrence and Compo (1998) empirically computed a reconstruction coefficient of $C_\delta = 0.776$ with $M_N = 6$. Numerical evaluation shows the product $NC_\delta \sim 2$, and the reconstruction approximation for the analytic (Appendix F) quantum wavelet of arbitrary order is

$$g_{\mathbb{C}}[m] \approx \frac{\pi^{\frac{1}{4}}}{2} \sum_{n=0}^{Np-1} \frac{\mathcal{W}_n[m]}{\sqrt{s_n}}$$

It is important to note how substantially different this expression is to the inverse discrete Fourier transform, where

$$g_{DFT}[m] = \frac{1}{\sqrt{Np}} \sum_{n=0}^{Np-1} \hat{g}_{DFT}[n] \, exp(j2\pi mn/Np)$$

where $\hat{g}_{DFT}[n]$ are the Fourier coefficients. Unlike the discrete Fourier transform, the standard wavelet reconstruction does not require multiplication by the mother wavelet. However, in the special case where the atoms are well matched to the signal of interest, it of interest to consider the sparse set of coefficients corresponding the complex time indexes $m_{n\,\mathbb{C}\,max}$ of the maximum energy, entropy, or SNR at each scale

$$g_{\mathbb{C}}[m] \approx \frac{\pi^{\frac{1}{4}}}{2} \sum_{n=0}^{Np-1} \frac{\mathcal{W}_n[m_{n\,\mathbb{C}\,max}]}{\sqrt{s_n}} Re\{\Psi_n[m - m_{n\,\mathbb{C}\,max}]\}$$

where the maximum indexes have to be computed separately for real and imaginary components. This has the form of a sum over the dominant Gabor atoms for each scale. Since one is only considering the maxima in a given record window, this is a very sparse representation consisting of the coefficient and the time offset corresponding to the peak energy or entropy estimate. Numerical evaluation shows that this expression can be used to estimate the full analytic function representation as long as reconstruction uses only the real atom function as the time shifts in the Hilbert transform already include the $\pi/2$ time shift.

6. Wavelet Information and Entropy

One advantage of the constant Q wavelet representation is that it is possible to estimate the information content and detectability of a signal in a band by applying the same set of wavelet transforms to the signal and comparing them to the transform of a noise segment or model. Consider the definition for Shannon's channel capacity, with

$$SNR_n = \frac{Ns_n + Sg_n}{Ns_n} = 1 + \frac{Sg_n}{Ns_n}$$

$$Ch_n = W log_2(SNR_n)$$

where Sg is the wavelet-transformed signal power and Ns is the wavelet-transformed noise power in a band. I consider two possible estimates for the bandwidth W. The first estimate approximates W by the ½ power point (-3dB) bandwidth

$$\Delta f_n = \frac{f_n}{Q_N} \approx \frac{1}{\sqrt{2}} \frac{f_n}{N} \approx 0.7071 \frac{f_n}{N}$$

The second estimates W using the Gabor box standard deviation for the angular frequency

$$\sigma_\omega = \frac{1}{\sqrt{2}} \frac{\omega_n}{M_N} \approx \frac{1}{4\sqrt{ln2}} \frac{\omega_n}{N} \approx \frac{\pi}{2\sqrt{ln2}} \frac{f_n}{N} \approx 1.8867 \frac{f_n}{N}$$

so that

$$\sigma_f = \frac{\sigma_\omega}{2\pi} = \frac{1}{4\sqrt{ln2}} \frac{f_n}{N} \approx 0.3003 \frac{f_n}{N}$$

Taking the average of Δf_n and σ_f

$$Ch_n \approx \frac{1}{2} \frac{f_n}{N} log_2(SNR_n)$$

The effective SNR_G and therefore the "detectability" of a bandwidth-limited compressed pulse (Berg and Pellegrino, 1996) can be represented by the product of the Gabor time-bandwidth product (Appendix C) and the signal to noise ratio

$$SNR_G = \sigma_t \, \sigma_\omega \times SNR_n$$

Since the time-bandwidth product for the Gaussian wavelet is constant

$$\sigma_t \sigma_w = \frac{1}{2}$$

and the uncertainty of its Gabor box is at the minimum, the likelihood of the detection of a SOI in a given band n is only proportional to its SNR.

Shannon's definition of the channel capacity was intended to represent the highest theoretical transfer rate of information through an analog line. Since SNR is given in power, which is typically the square of the signal amplitude, an unscaled binary log is off by a factor of two. To reconcile this definition with the original collection of a time series signal in floating point bits (fbits), I define the binary SNR to match the signal rms amplitude as well as Shannon's units for the information rate per band $Ch_{N,n}$ of the Quantum compressed pulse as

$$bSNR_n = \frac{1}{2} log_2(SNR_n) = log_2(\sqrt{SNR_n}), \quad fbits$$

$$Ch_{N,n} = \frac{f_n}{N} \times bSNR_n, \quad shannons = fbits/s$$

The increase in higher information delivery rate with increasing frequency is intuitive as more cycles are transferred per second. As the order number increases, the bandwidth narrows and so the potential information rate decreases. Less obvious is the decrease in high-frequency information with increasing distance in a lossy transmission channel. Assuming the noise power remains unchanged, the decrease in

SNR with increasing scaled distance r from the source origin on a lossy acoustic channel can be represented as

$$SNR = SNR_o \frac{exp(-\gamma f^2 r)}{r^{n_g}}$$

Where $n_g = 2$ for spherical geometric spreading in free space and $n_g = 1$ for cylindrical spreading in a waveguide. The binary SNR can be represented as

$$SNR = \left[bSNR_0 - \frac{n_g}{2} log_2 r \right] - f^2 r \, (\gamma \, log_2 e)$$

The term in parenthesis shows the expected reduction of one bit per doubling of distance for spherical spreading $(n_g = 2)$. The last term suggests the frequency dependence of the channel capacity in a lossy acoustic medium may have the general form

$$Ch_n \sim \alpha(log_2 r) \, f - \beta(r) \, f^3$$

so that with increasing range the optimal information transmission frequency shifts to lower frequencies. One may readily extend the binary SNR definition to the measure of relative power

$$bR = log_2 \left(\sqrt{\frac{S}{S_{max}}} \right) = \frac{1}{2} log_2 \left(\frac{S}{S_{max}} \right), \quad fbits$$

so that the -3dB half-power point becomes the -1/2 bit power point.

The entropy of a signal of interest can be estimated by the wavelet coefficients. A practical approach is described in Li and Zhou (2016). The information content of each scale n at the time step m can be estimated from the wavelet energy. I first estimate

$$E_{m,n} = \left| Re\{ \mathcal{W}_{m,n} \} \right|^2 + j \left| Im\{ \mathcal{W}_{m,n} \} \right|^2$$

the total energy in a given record can be estimated from

$$E = \sum_m \sum_n \sqrt{E_{m,n} E_{m,n}^*}$$

The probability of $\mathcal{W}_{m,n}$ in the record is

$$p_{m,n} = \frac{E_{m,n}}{E}$$

where

$$\sum_m \sum_n p_{m,n} \, p_{m,n}^* = 1$$

The log energy entropy (lee) per coefficient can be defined buy the binary logarithm

$$e_{lee} = log_2 \left(p_{m,n}^2 \right) = 2 log_2 \left(p_{m,n} \right)$$

Where it should be noted that the factor of two scaling coefficient does not alter the relative weight of each coefficient. The Shannon entropy (se) per CWT coefficient is defined as

$$e_{se} = -p_{m,n} log_2(p_{m,n})$$

with corresponding complex versions that separate the real and imaginary components. These entropies can be readily evaluated to construct noise models from the lowest entropy components. If a stable noise model can be constructed from the record or from prior knowledge of the environment and transmission channel, SNR estimates can be computed and the process repeated to evaluate the dimensionless binary log of the SNR

$$bSNR_{m,n} = \frac{1}{2} log_2(SNR_{m,n})$$

and the product of the ratio and the binary ratio (RbR), an entropy-like nondimensional metric of the SNR that can be readily evaluated to identify and extract the wavelet coefficients would be most representative of a signal of interest,

$$RbR_{m,n} = SNR_{m,n} \times bSNR_{m,n}$$

7. Praxis: One Ton Blast

Consider a normalized transient wave function characteristic of chemical or nuclear explosives. Suppose one wanted to construct a family of wavelets centered around 6.3 Hz, corresponding to the detonation of one metric ton on TNT. It is known that at some distance from the source this center frequency may drop by an octave (factor of two in frequency) or more, as well as become stretched out (dispersed) in time due to propagation effects. A theoretical source pressure function for the detonation of high explosives was developed in some detail in Garces (2019) and is used here to construct a representative synthetic.

Let $\hat{t} = \frac{t}{\tau_p} = 4\frac{t}{\tau_c}$, where $\tau_c = 4\tau_p$ is the pseudo-period of a blast pulse corresponding to the peak spectral energy and τ_p is the duration of the positive blast phase. The form of the amplitude-normalized source pressure function (Garces 2019) is represented as

$$g(\hat{t}) = (1 - \hat{t}), \quad 0 \le \hat{t} \le 1$$

$$g(\hat{t}) = \frac{1}{6}(1 - \hat{t})(1 + \sqrt{6} - \hat{t})^2, \quad 1 < \hat{t} \le 1 + \sqrt{6} .$$

This pulse has an associated analytical function $g_{\mathbb{C}}(\hat{t})$ as discussed in Appendix G. Since the theoretical Hilbert transform has some unresolved issues, I also use the numerical Hilbert transform provided by the Scipy function signal.hilbert for comparison.

Note the amplitude is not used in this exercise as in cyber-physical systems such as smartphones the amplitude response of on-board sensors may not be known. However, sensor dynamic range is usually specified and available (e.g. int16, float32) and can be used for signal scaling relative to the full range or the noise.

The normalized pulse has zero mean (conservation of momentum) and its theoretical variance is

$$\sigma_p^2 = \int_{-\infty}^{\infty} g^2(\hat{t}) \, dt = 0.95 \frac{\tau_c}{8}$$

The complex Fourier transform $\hat{g}(j\hat{\omega})$ of this pulse is

$$\hat{g}(j\hat{\omega}) = \frac{\pi}{2\omega_n}\left[\frac{1 - j\hat{\omega} - e^{-j\hat{\omega}}}{\hat{\omega}^2} + \frac{e^{-j\hat{\omega}(1+\sqrt{6})}}{3\hat{\omega}^4}\left\{j\hat{\omega}\sqrt{6} + 3 + e^{j\hat{\omega}\sqrt{6}}[3\hat{\omega}^2 + j\hat{\omega}2\sqrt{6} - 3]\right\}\right]$$

where $\hat{\omega} = \frac{\pi}{2}\frac{\omega}{\omega_c} = \frac{\tau_c}{4}\omega = \tau_p\omega$ and the peak in the spectrum is at $\omega = \omega_c$. Note there are at least two pseudoperiods of importance evident in the main blast pulse: the main spectral pseudoperiod τ_c and positive phase pseudoperiod of $2\tau_p$. Near the source the positive phase pseudoperiod will dominate as it has the highest energy and bandwidth. With increasing distance and high-frequency attenuation the main pseudoperiod becomes more prominent and may also be downshifted in frequency (Garces, 2019). However, additional scales can be introduced by reflection and refraction in the transmission channel that can induce phase shifts often modeled with Hilbert transforms (Appendix G).

The power spectra of real digital signals are usually expressed using only the positive frequencies up to the Nyquist frequency, where the unilateral spectral density $Pg(\hat{\omega})$ is defined as

$$Pg(\hat{\omega}) = 2|\hat{g}(j\hat{\omega})|^2 = 2\,\hat{g}(j\hat{\omega})\hat{g}^*(j\hat{\omega})$$

Since the target signature corresponds to a one tonne (1000 kg) blast, the analysis concentrates on a target frequency of 6.3 Hz (Garces, 2019),

$$f_{tg} = 6.3\text{Hz}$$

The general procedure for constructing target-tuned fractional binary bands of order N is to define a set of base-2 scales

$$f_j = f_{tg}2^{\frac{j}{N}}$$

The upper limit is set by the Nyquist frequency

$$f_{j\,max} = f_{tg}2^{\frac{j\,max}{N}} < \frac{f_s}{2} \Rightarrow j\,max < floor\left(Nlog_2\left[\frac{f_s}{2f_{tg}}\right]\right)$$

The lower limit is set by the largest data window duration T

$$f_{j\,min} = f_{tg}2^{\frac{j\,min}{N}} > \frac{2}{T} \Rightarrow j\,min > ceil\left(Nlog_2\left[\frac{2}{Tf_{tg}}\right]\right)$$

so the center frequencies are defined by

$$f_j = f_{tg}2^{\frac{j}{N}}, \quad j \in [j\,min, j\,max]$$

which will be sufficient information to compute the Morlet scale s_n. If one must convert to a sorted, monotonically increasing pseudoperiod, let

$$\tau_j = \frac{1}{f_j}, \quad \tau_0 = min(\tau_j)$$

And restart the counter for the period

$$\tau_n = \tau_0 2^{\frac{n}{N}}, \quad n \in [0, j\,max - j\,min = length\,(f_j)]$$

For the purposes of illustration, let's choose a signal frequency that exactly matches the target frequency; if this example fails there is no purpose in continuing. This would correspond to

$$f_c = f_{tg} = 6.3 \text{Hz}$$

in the GT pulse. A sample rate of 200 Hz will be more than sufficient for this example. I add gaussian noise with a standard deviation that is one bit below the signal variance (factor of 1/2), and then anti-alias filter all frequencies below Nyquist. The analytic function is computed numerically from the real pulse for later comparisons with the wavelet-reconstructed signal.

The CWT scalogram is computed using the complex nondimensional mother quantum wavelet of order N. The complex Gabor-Morlet wavelet in Scipy is represented by the function scipy.signal.morlet2, and has the desired canonical form,

$$\Psi_H(m) = \frac{1}{\pi^{1/4}} exp\left(-\frac{m^2}{2}\right) \exp\left(iM_N m\right)$$

$$\Psi_{u,n}(m) = \frac{1}{\sqrt{s_n}} \Psi_H\left(\frac{m-u}{s_n}\right)$$

$$s_n = s_0 \, 2^{\frac{n}{N}} = \left[\frac{M_N}{2\pi} f_s \tau_0\right] 2^{\frac{n}{N}} = \frac{M_N}{2\pi} \frac{f_s}{f_n}$$

$$T_n = [M_N \tau_0] 2^{\frac{n}{N}} = \frac{M_N}{f_n}$$

$$M_N = 2\sqrt{ln(2)} \, Q_N$$

$$Q_N = \left[2^{\frac{1}{2N}} - 2^{-\frac{1}{2N}} \right]^{-1}$$

The only free variables are the order N, the smallest time scale τ_0, and the sample rate f_s. The nominal number of points per window can be estimated from $f_s T_n$. The complex wavelet coefficients can be readily computed from the real part of the discrete version of the blast source-time function $p(m)$

$$\mathcal{W}_n[m] = \sum_{m'=0}^{Mp-1} p(m') \Psi_n^*(m' - m) = p \circledast \Psi_n^*[m]$$

I use the SciPy cwt function, which in turn invokes the convolution function. This is computationally expensive: we've turned a time series with Mp points into a complex 2[Mp x Nbands] array of band-passed waveforms. The terms wavelets and wavelet filter banks are often used interchangeably in the context of the CWT.

The wavelet-filtered reconstructed complex analytical signal can be approximated from

$$g_{\mathbb{C} \, ij}[m_k : m_l] \approx \frac{\pi^{\frac{1}{4}}}{2} \sum_{n=i}^{j} \frac{\mathcal{W}_n[m_k : m_l]}{\sqrt{s_n}}$$

Where the i, j indexes indicate that one may choose selected scales for the reconstruction over selected time indexes $m_k : m_l$ corresponding to the wavelet coefficients that best represent a signal of interest during the time interval of relevance. The scaled wavelet coefficients for an binary band decomposition are shown in Figure 1, and Figure 2 shows a comparison of the input synthetic analytic record and the

analytic signal reconstruction (summed over all scales) for the octave band representation. In Figure 1 the CWT wavelet amplitudes are scaled by the reconstruction coefficients.
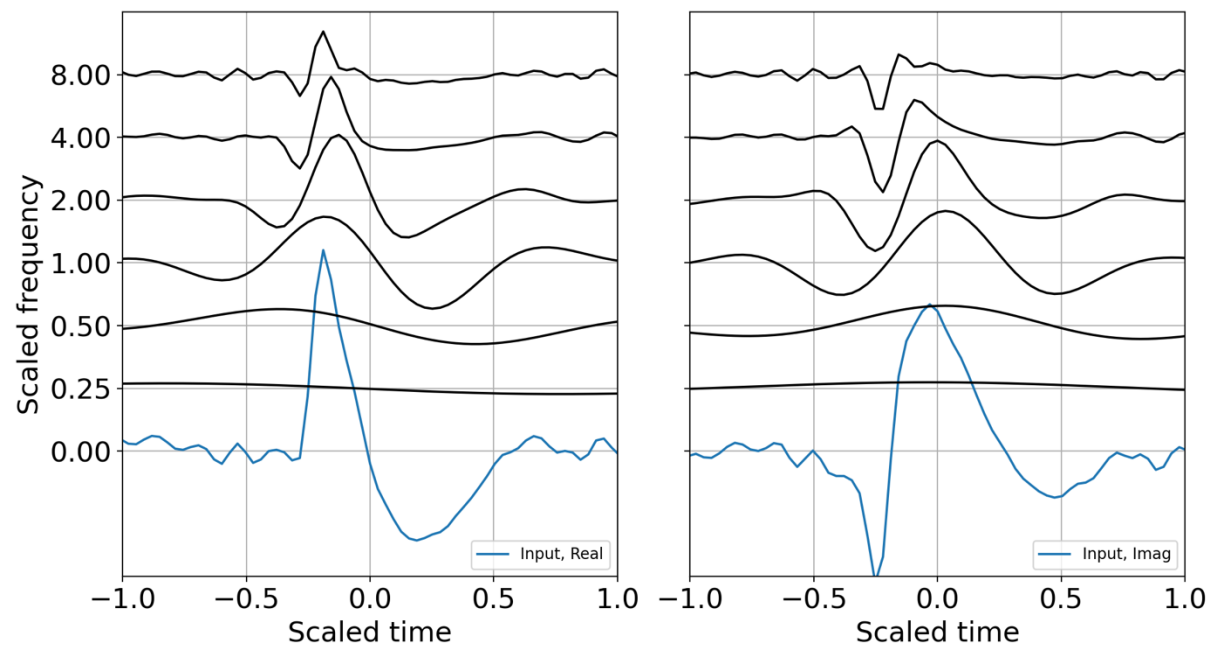
Figure 1. Analytical signal from mathematical equation, computation with SciPy Hilbert, and the CWT reconstruction. (**a**) Real part; (**b**) imaginary part. The wavelets were evaluated in binary bands (N=1) and constructed around the target frequency of 6.3 Hz, which scales frequency and time. The real input waveform and its computed Hilbert transform are displayed in blue at the zero frequency.
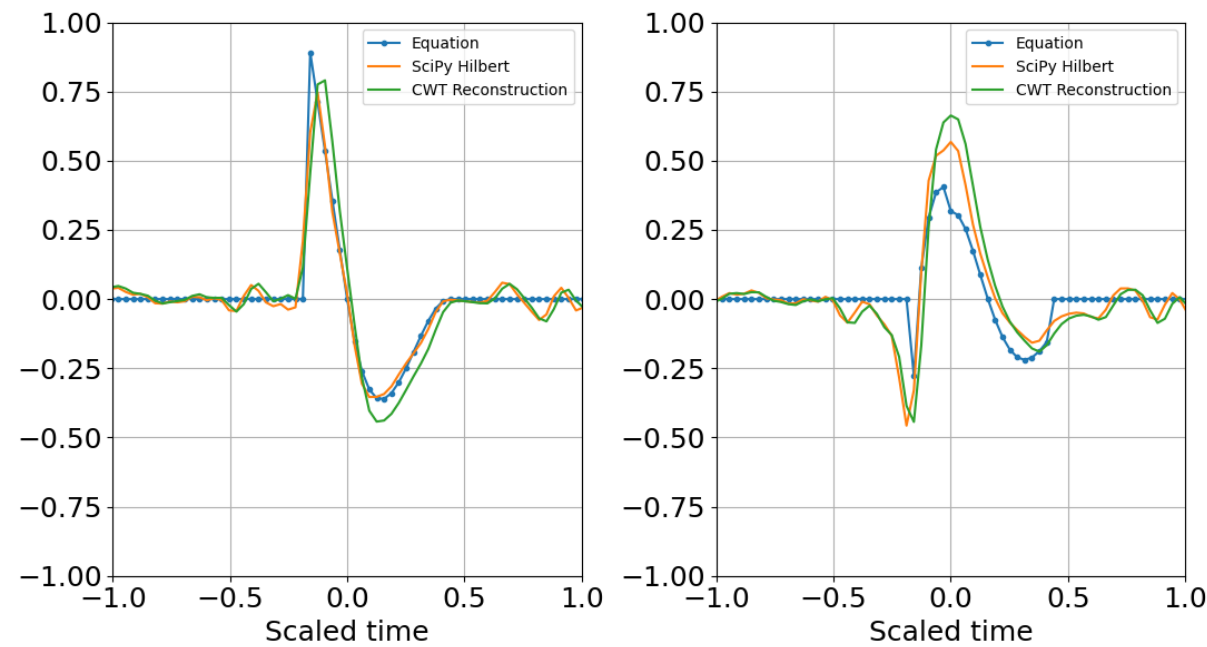
Figure 2. Wavelet reconstruction with binary bands. (a) Real part; (b) Imaginary part. The Equation waveform has no noise and is not filtered, whereas Hilbert has Gaussian noise and has been anti-aliased filtered.

The reconstruction process recovers the original dimensionality of the time series but returns its Hilbert transform, so the total dimensionality may be doubled (2Mp sample points). If only the original real signal is desired, then the dimensionality is unchanged.

I next proceed to the estimation of entropy, SNR, and consider sparse signal representation. Although binary bands are adequate for characterizing this signal, and are routinely used in the discrete wavelet transform, I take advantage of the flexibility offered by the CWT and use third order bands (N=3) for the examples that follow. One of the benefits of order 3 bands is that the admissibility condition is better met and scales are recursive in powers of 2 and 10 (e.g. Garces, 2013). As presented in Appendix E, third order bands will contain over 99% of the Gabor box variance within an octave and within 80% of the full window T_n, reducing spectral leakage. If, in addition, one wants a factor of two accuracy in explosive yield estimates, 1/3 octave resolution is a minimum requirement. A third order band wavelet decomposition is presented in Figure 3, and is the equivalent of the scalograms usually represented as color plots. I choose the wire mesh representation to better illustrate the simplicity of the CWT decomposition. The difference between Figure 3 and Figure 5 is that the first scales the raw CWT coefficients by the reconstruction scaling, whereas Figure 5 shows the raw coefficients.
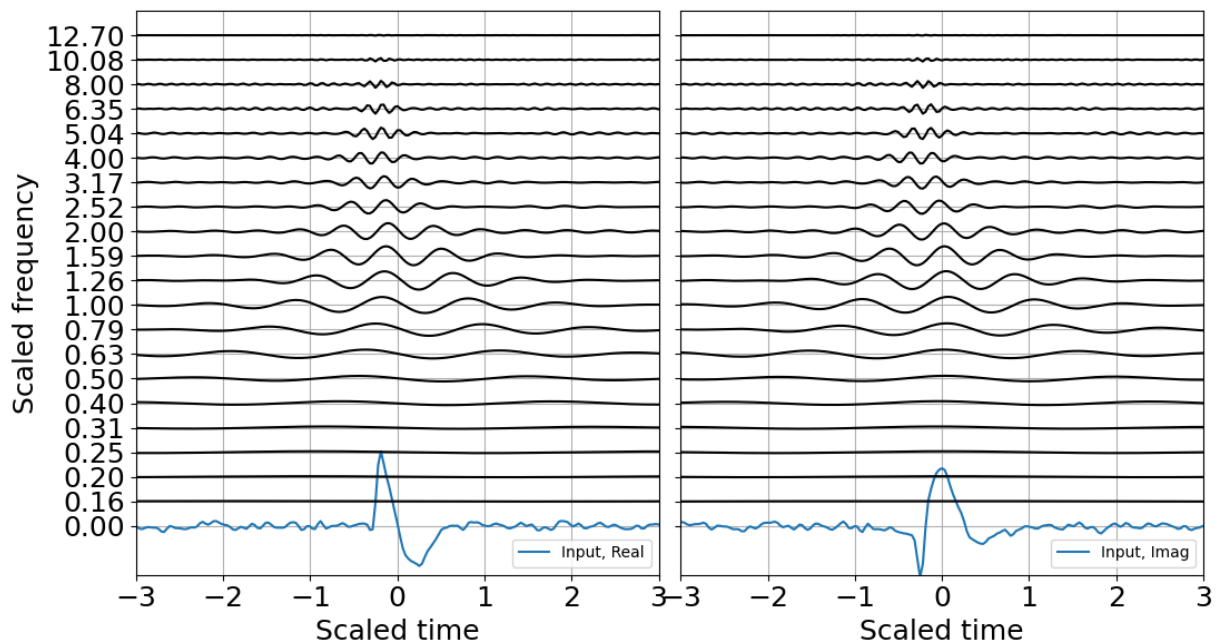
Figure 3. Wavelet decomposition with 1/3 octave bands, with CWT amplitudes scaled by the reconstruction coefficients. (a) Real part; (b) Imaginary part. As with Figure 1, the input waveform is displayed at the zero frequency.
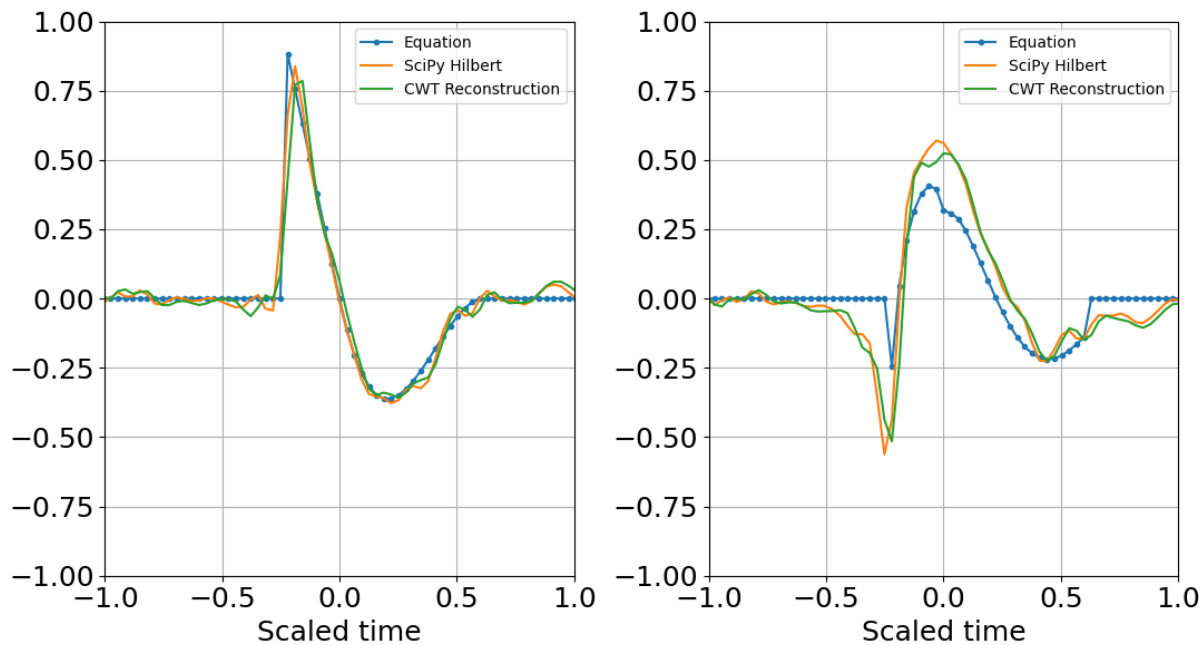
Figure 4. Wavelet reconstruction with 1/3 octave bands. (a) Real part; (b) Imaginary part.
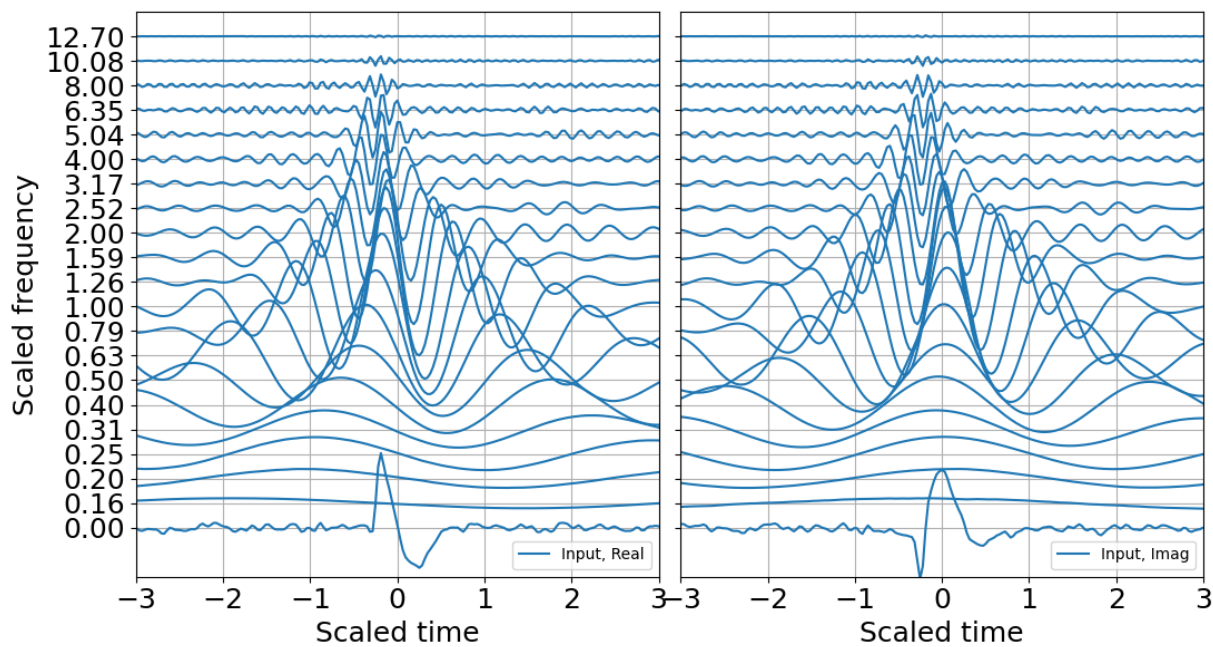
Figure 5. Wavelet decomposition in order 3 binary bands, raw CWT amplitudes. (a) Real part; (b) Imaginary part.

The energy probability distribution is constructed from the wavelet coefficients to estimate entropy, as discussed in the previous section. The log energy entropy looks like any other scalogram and does not

add much value, but the Shannon entropy plot is interesting and well scaled (Figure 6). The peak entropy is at the blast center frequency, as expected.
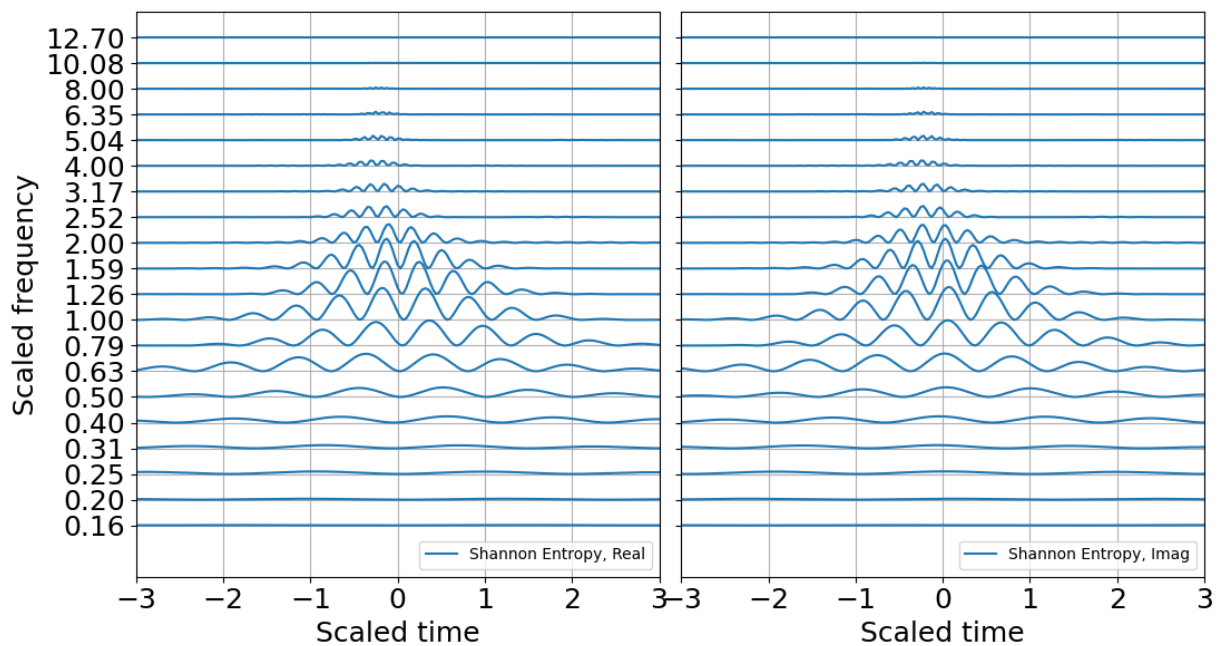
Figure 6. Shannon entropy in order 3 bands from raw CWT amplitudes. (a) Real part; (b) Imaginary part.

Next I construct a noise model to build the SNR, and to establishing criteria for standardized and reproducible sparse signal representation. Many are the ways to characterize noise, and few of them accurately characterize non-stationary noise over brief observation windows. An incorrect noise model can penalize the signal passband and degrade the signal SNR. For the white noise model with variance that is one bit below the signal variance, the CWT of the noise (Figure 7) shows how the high-frequency oscillations are adequately sampled whereas the low-frequency oscillations are undersampled. This leads to instability if the noise is only estimated over a brief observation record. In principle once can build a noise model over a substantial period of time to obtain better statistical significance under the assumption the noise is stationary. This can be a tenuous assumption in some circumstances. Noise studies are beyond the scope of this paper, and to estimate noise I flatten the noise spectrum by using the mean of the noise coefficients of the over all bands.
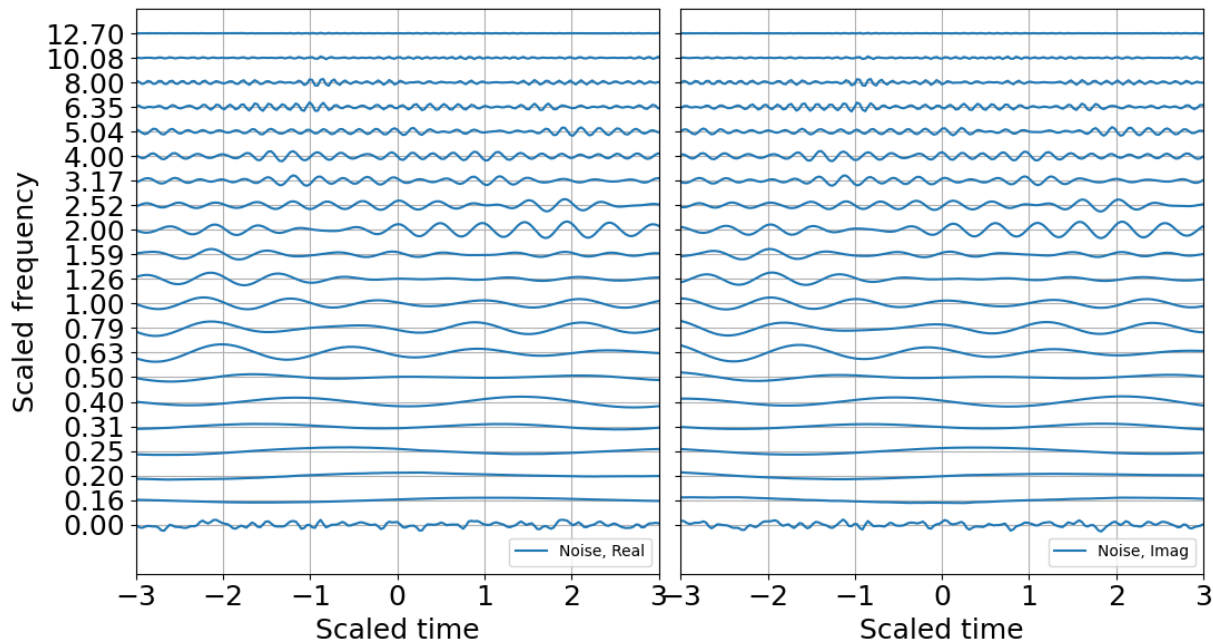
Figure 7. Raw CWT of noise in 1/3 octave bands. (a) Real part; (b) Imaginary part.

The expected binary SNR would look much like the log energy entropy as they are both scaled by a constant value, the former over the average noise and the latter over the total energy. The SNR RbR, as described in the previous section, should also look very much like the entropy, except it would be zero for SNR of unity and positive for SNR>1. The SNR RbR is shown in Figure 8, and unsurprisingly, matches the Shannon entropy plot. These are good news; the entropy plot requires constructing an energy distribution that scales with the record, whereas the SNR requires constructing a noise model that is mostly independent of the record and should have more stability as long as the ambient noise is approximately stationary or can at least be adequately modeled. If one is curating data for machine learning training, the entropy would be a good metric for picking and annotating, as well as for refining noise models. If one is trying to trigger or detect signals operationally, the SNR may be a preferable metric as it makes no assumptions about the total energy in a record and only scales relative to a (preferably) stable noise representation.
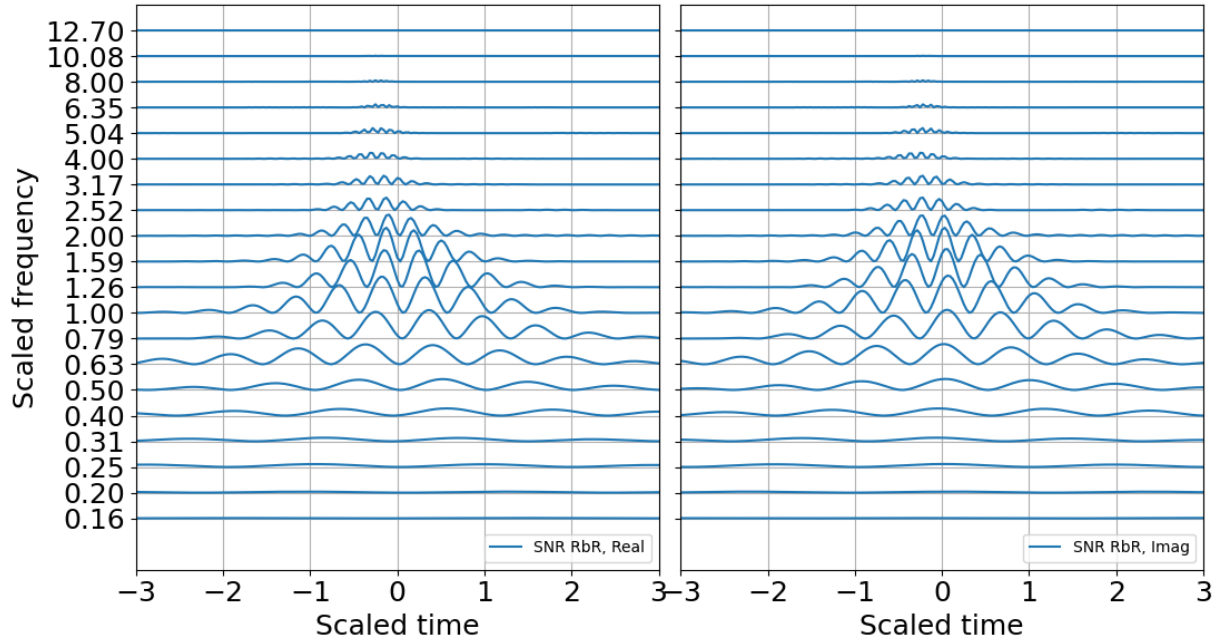
Figure 8. SNR RbR in 1/3 octave bands. (a) Real part; (b) Imaginary part.

We can use the CWT coefficient energy, the Shannon entropy, or the SNR RbR test the feasibility of the sparse Gabor atom superposition. Suppose we use any of these Np scales x Mpoint time matrices to identify the peak contributions over the record, and identify the complex time indexes as $m_{\mathbb{C}\,max}$. The quantum wavelet superposition would be expressed as

$$g_{\mathbb{C}\,ij}[m_k:m_l] \approx \frac{\pi^{\frac{1}{4}}}{2} \sum_{n=i}^{j} \frac{\mathcal{W}_n[m_{n\,\mathbb{C}\,max}]}{\sqrt{s_n}} Re\{\Psi_n[m_k:m_l - m_{n\,\mathbb{C}\,max}]\}$$

where the dimensionality of the representation is reduced to the complex coefficients and time indexes. Since the wavelet function can be reproduced for any time index, the time array need not be stored. In other words, if there are 20 scales, there will be 20 real coefficients and time offsets and 20 imaginary coefficients and time offsets, with total dimensionality of 4x20 = 80 parameters. If there is sufficient SNR and the signal is band limited it is possible to further reduce dimensionality by removing any coefficients below a specified threshold that may be fitting to noise (e.g. overfitting). Figure 9 shows the result of reconstruction from the superposition of all the top atoms of the 20 scales, and Figure 10 shows reconstruction from a sparser set of 12 scales with the highest SNR RbR. Similar results were obtained using the Shannon entropy. The Gaussian noise standard deviation for these two runs was one bit below the signal standard deviation.
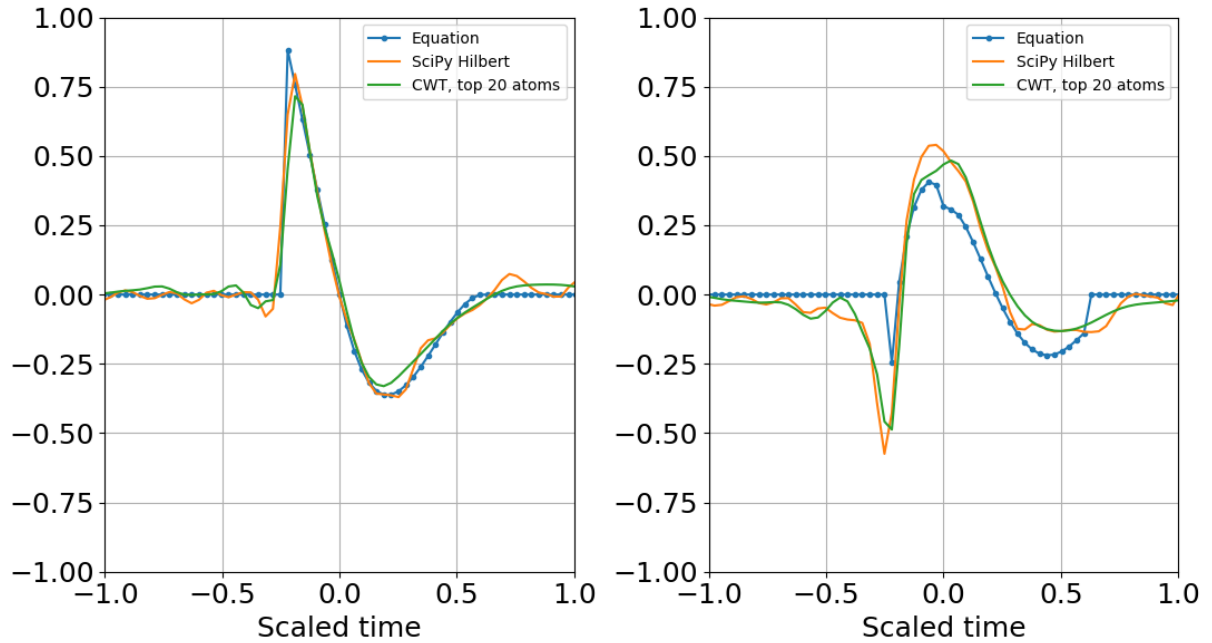
Figure 9. Superposition of largest SNR entropy coefficients per band using all twenty 1/3 octave bands. (a) Real part; (b) Imaginary part. The noise standard deviation is one bit below the signal's. Dimensionality is reduced to the number of coefficients and their corresponding time shifts.
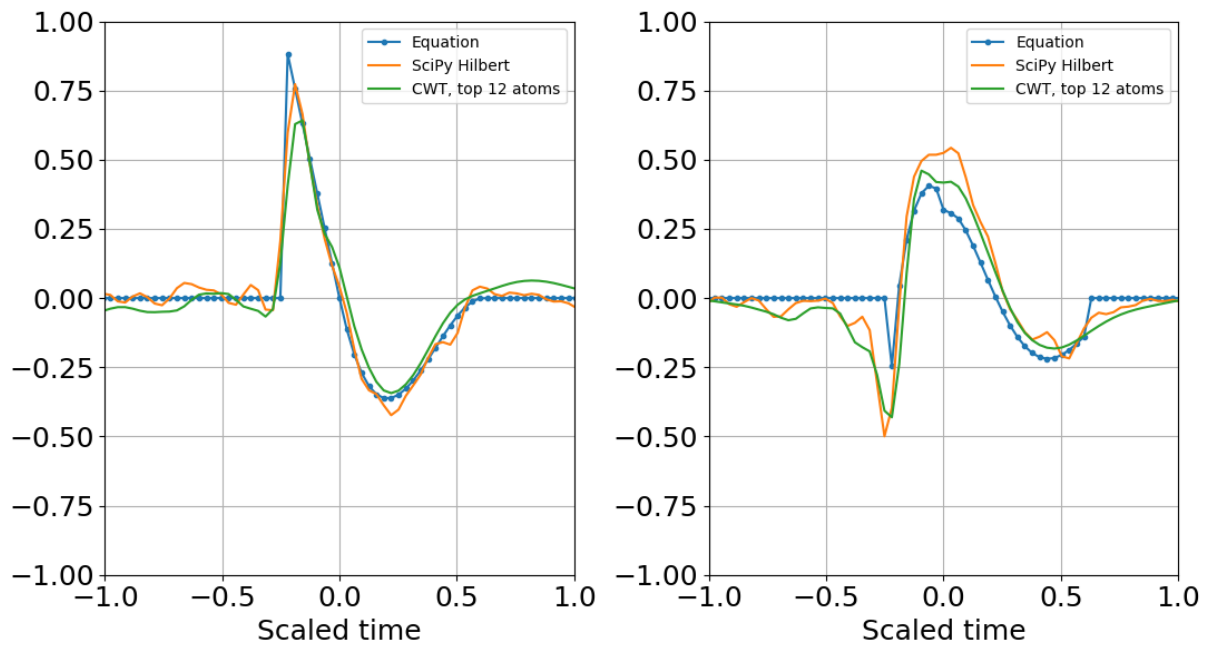
Figure 10. Superposition of largest coefficients per band within 4 bits of the peak SNR entropy. (a) Real part; (b) Imaginary part. Dimensionality is further reduced by applying the cutoff.

Increasing the noise standard deviation by a factor of two (one bit) still permits reconstruction from superposition (Figure 11), and increasing by another bit also allowed atomic reconstruction (Figure 12).
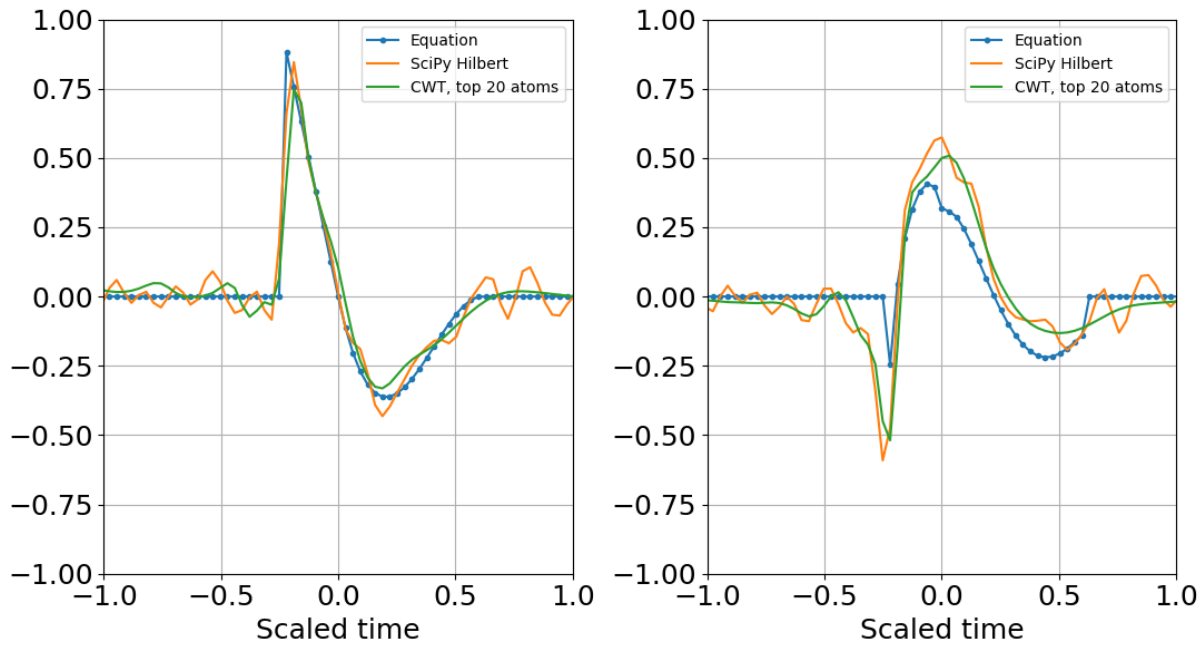
Figure 11. (a) Real part and (b) imaginary part of the original and reconstructed waveform. Increasing the noise amplitude so that its variance is the same as the signal variance still permitted reconstruction from the superposition of the largest atoms per band.
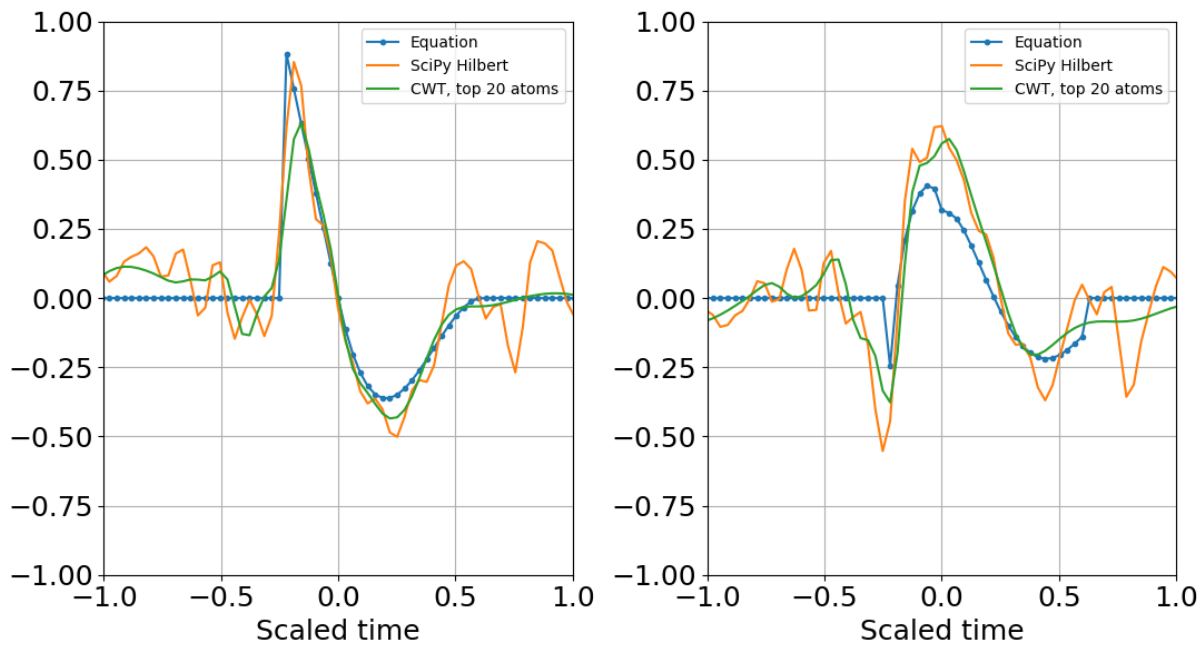
Figure 12. (a) Real part and (b) imaginary part of the original and reconstructed waveform. Increasing the noise standard deviation is one bit above the signal standard deviation also allowed reconstruction from the quantum wavelet superposition.

There is no end to the number of sensitivity studies that can be performed; in addition to other SNR test I also shifter the peak blast frequency from the target frequency and could still get stable reconstruction.

Increasing the order past N>6 only worsened the fit to the target waveform so it only increases dimensionality and computational cost with a decrease in reconstruction fidelity, as is to be expected from using a wavelet that does not match the target signature.

5. Coda

This paper proposes a transition to binary metrics for digital data and introduces a standardized, quantized variation of the Gabor atoms with binary bases, optimal time-frequency resolution, and clear spectral energy containment. A binary entropy-like metric for the SNR is proposed and used to extract the peak coefficients to evaluate the performance of the superposition of Gabor atoms against the more traditional CWT reconstruction. Although the immediate application is the analysis of time series data collected with cyber-physical systems such as smartphones, the methods presented in this paper should be transportable to other types of digital records and can be extended to other wavelet families.

I used a synthetic for a 1 tonne detonation in Gaussian noise as an example, and did not include the blast amplitude as a key parameter so as to concentrate on the entropy and SNR, both which are dimensionless scaled quantities. Observations collected close to an explosion should have brief durations and a high SNR; for short pulses it is advisable to use smaller orders (N=1-6) Gabor atoms. Due to cube root yield scaling, the third order bands will provide factor of two yield resolution, and one-sixth order bands a factor of square root of two yield resolution. Acceptable signal reconstructions were obtained from the CWT coefficients as well as the superposition of the peak 3rd order Gabor atoms for the blast signature.

At increasing distance from the source the peak frequency is expected to drop (e.g. Garces, 2019) and the pulse disperses to spread out in time. This opens up the possibility for stable 6 and 12 order analyses with a corresponding improvement in yield resolution. Future work will concentrate on such dispersed signatures as well as consider other types of CW signatures that would be well matched to higher-order Gabor atoms.

The methods developed have the goal of providing a tunable, standardized framework for signature feature extraction to be used for signal classification (e.g. Shi and Zhang, 2001), and should be well suited for dictionary learning (e.g. M9).

Note to Reviewers:
The appendices that follow span over ~5 years and may have different notations than the main body of the text. They are provided as to facilitate verification and will be cleaned up after the review process.

Appendix A. Generalized Constant Q Bands

Logarithmic constant-bandwidth, also referred to as proportional frequency or constant quality factor (Q) bands, are traditionally defined by their scaled bandwidth

$$\frac{\Delta f}{f_c} = \frac{f_H - f_L}{f_c} = \frac{1}{Q}$$

where f_c is the center frequency and f_H and f_L are referred to as the upper and lower band edge frequency, respectively. Note that it is also possible to use angular frequencies, where $\omega = 2\pi f$ and

$$\frac{\Delta \omega}{\omega_c} = \frac{2\pi(f_H - f_L)}{2\pi f_c} = \frac{1}{Q}$$

If we define the center, upper, and lower band edge *periods* as

$$\tau_c = \frac{1}{f_c}, \ \tau_H = \frac{1}{f_L}, \ \tau_L = \frac{1}{f_H}, \qquad f_c^2 = f_L f_H$$

Then

$$\frac{\Delta \tau}{\tau_c} = \frac{\tau_H - \tau_L}{\tau_c} = \frac{\Delta f}{f_c} = \frac{\Delta \omega}{\omega_c} = \frac{1}{Q}$$

The reader can verify that the same logic would apply to a scalar wavelength and wavenumber. In this section we generalize the constant-Q framework to the logarithmic discretization of evaluation intervals relative to a given reference scale and base. For a given reference scale S_0, which could be time, frequency, spatial length, wavenumber, or any other useful metric, we define a logarithmic scale base $G > 1$ and center scale S_C as

$$\frac{S_C}{S_0} = G^{\frac{n}{N}}$$

where n is the band number and N is the band order, subject to the constraints $n \in \mathbb{Z}, \ N \geq 1$. This section provides a higher-level abstraction to the equation in the main text, where

$$\tau_n = S_C$$

The upper (S_H) and lower (S_L) band edge scales are defined relative to the center scale by

$$\frac{S_H}{S_C} = G^{\frac{1}{2N}}, \qquad \frac{S_L}{S_C} = G^{-\frac{1}{2N}}, \qquad \frac{S_H S_L}{S_C^2} = 1$$

with constant quality factor Q_N, or constant proportional bandwidth,

$$\frac{1}{Q_N} = \frac{S_H - S_L}{S_C} = G^{\frac{1}{2N}} - G^{-\frac{1}{2N}} \ .$$

Note that center and band edge scales attached to a given band n change with the order N, reference scale S_0, and the reference base G.

The next step substantially simplifies the implementation of constant-Q bands with a minimal introduction of a 2% computational error. To the author's knowledge, this is the first time this expression

is presented (and he would be most grateful to be informed otherwise). Numerical evaluation showed that:

$$\lim_{N\to\infty}\frac{Q_N}{Q_1} = \lim_{N\to\infty}\left(G^{\frac{1}{2}} - G^{-\frac{1}{2}}\right)\left(G^{\frac{1}{2N}} - G^{-\frac{1}{2N}}\right)^{-1} \approx N\frac{G-1}{\sqrt{G}\,ln(G)} \approx (1.02\,)N \approx N$$

$$Q_N \approx NQ_1 = N\left[\frac{\sqrt{G}}{G-1}\right]$$

The center frequencies and band edges, and thus the quality factor, of traditional fractional octave bands are well known and can be readily computed for all the standard bands. The primary value of the expression for Q_N is that it provides a simple, explicit estimate of the relation between the quality factor and the band order, which is turn permits an estimate of the support window duration for a given wavelet in terms of the band order. Numerical inspection shows that for most practical applications and for $G = 2 \approx 10^{\frac{3}{10}}$, even those when N is non integer, we can use the expression

$$Q_N = Q_1 N = \sqrt{2}N$$

to numerically evaluate the relationship between the band order and the quality factor. It is very unlikely that a constant-Q bands will be requested for $Q_N < 1$ as there should be at least one oscillation in a Gabor wavelet. The special case $Q_N = 1$ leads to a fractional order $N_1 = \frac{1}{\sqrt{2}} \approx 0.707$ and a set of oddly spaced center frequency bands.

As an extension of Garces (2013), a standardized set of scales S_G may be defined as a multiple M_G of the scale as

$$S_G(N,n) \stackrel{\text{def}}{=} M_G S_c = M_G S_0 G^{\frac{n}{N}}$$

This expression is explicit in expressing evaluation scales as a function of the Gabor window for each order and band number n, but is still relatively unconstrained in the selection of the Gabor scale multiplier M_G. Although previous implementations have used M_G as powers of two of the Gabor window S_G as initial values, the final value of the multiplier may depend on the selected window optimization algorithms.

Appendix B. The Gabor Wavelet

Different disciplines call the same things different names; many of the challenges in present-day data science are often due to divergent lexicon and the diversity of applications specific to each field. The idea of using a windowed sinusoid as a basis function for signal representation was developed in detail in Gabor's 1946 landmark paper, where he also introduced the time-frequency uncertainty principle. Gabor's atoms were further developed by Grossman and Morlet (1984), and P. Goupillaud et al. (1984) (amongst others), who formalized and popularized what we now know as *wavelet* transforms. Mallat (2009) presents a lucid overview of the complementary nature of Fourier and wavelet representations in his Wavelet Tour of Signal Processing, and is used as a primary reference. Mallat (2009) is referenced often in this paper and is hereafter referred to as M9; the serious student would be wise to consider it required reading.

The Gabor wavelet is a special case of a wavelet-modulated window (M9, Eqs. 4.60-4.62) and is representative of a bandwidth-limited compressed pulse (Berg and Pellegrino, 1996). For a physical scientist, its most intuitive form is

$$\Psi(t) = \frac{1}{[\pi\sigma^2]^{1/4}} exp\left(-\frac{t^2}{2\sigma^2}\right) exp\left(i\omega_c\, t\right),$$

representing a sinusoid with time t and angular frequency ω_c (or linear space and wavenumber) modulated by Gaussian window with standard deviation σ.

The Fourier transform of the mother wavelet is

$$\widehat{\Psi}(\omega) = [4\pi\sigma^2]^{1/4}\, exp\left\{-\frac{1}{2}\sigma^2[\omega - \omega_c]^2\right\},$$

has unit second moment

$$\int_{-\infty}^{\infty} \Psi(t)\psi^*(t)dt = 1\ ,$$

and it first moment vanishes in the limit

$$\int_{-\infty}^{\infty} \Psi(t)dt\ \to 0 \text{ for } \ \sigma^2\omega_c^2 \gg 1\ .$$

Another representation of the Gabor wavelet is

$$\psi(t) = \frac{1}{\sqrt{\pi 2\sigma^2}}\, exp\left\{-\frac{t^2}{2\sigma^2}\right\} exp\{i\omega_c t\}$$

With the advantage that its Fourier transform

$$\hat{\psi}(\omega) = \ exp\left\{-\frac{1}{2}\sigma^2[\omega - \omega_c]^2\right\}$$

has a peak amplitude of unity and yields equal-amplitude filter banks.

The computationally efficient forms of these wavelets are,

$$\Psi_{\mathcal{M}}(t) = \frac{1}{\pi^{1/4}}\, exp\left(-\frac{\eta^2}{2}\right) exp(iw\,\eta)$$

and

$$\psi(t) = \frac{1}{\sqrt{\pi b}}\, exp\left\{-\frac{t^2}{b}\right\} exp\{i\omega_b\, t\}$$

The term b is referred to as the bandwidth of the wavelet, although it is a misnomer as it will be found to be proportional to the inverse of the square of the angular bandwidth of a constant Q filter bank.

Mallat (2009) defines a wavelet dictionary as

$$\Psi_{u,n}(t) = \frac{1}{\sqrt{s_n}}\Psi\left(\frac{t - u}{s_n}\right)$$

$$\psi_{u,n}(t) = \frac{1}{s_n}\psi\left(\frac{t-u}{s_n}\right)$$

where s_n is a discrete set of wavelet scales that can be represented as

$$s_n = s_0 G^{\frac{n}{N}}, \quad s_0 \in \mathbb{R} > 0, \ G \in \mathbb{R} > 1, \ n \in \mathbb{Z}, \ N \in \mathbb{N}$$

These wavelet scale representation sets the stage for a constant-Q framework of order N. Additional properties of constant-Q scales are presented in Appendix A. Traditional constant-Q frameworks in acoustics and music applications match the 12-tone equal temperament system (N=12) for $G = 2$ or $G = 10^{\frac{3}{10}} \approx 2$ and are consistent with the Renard series recommended in ISO3 for N=1, 3, 6, 12, 24. This work builds on the Infrasonic Energy, Nth Octave (Inferno) formulation of Garces (2013) and expands to fractional orders. The Inferno multiresolution algorithm has also been implemented in infrasound array processing algorithms for nuclear monitoring applications (e.g. Vergoz et al, 2019; Mialle et al, 2019) However, the framework developed in this paper supersedes the work of Garces (2013); that young man had much to learn and took his time to do it.

The quantum variation of the Garbor-Morlet wavelet is constrained to constant-Q fractional bands that obey the relation

$$\sigma = \frac{M}{2\pi} = \frac{\sqrt{ln2}}{\pi}Q$$

where M is referred the scale multiplier as in Garces (2013).

Although the foundation of this work is general and can be readily expanded to spatial scales, the rest of this paper concentrates on time series applications, with examples in acoustics. Let s_n correspond to a time scale of interest τ_n. We can associate a pseudo-period in seconds with τ_n with a frequency f_n in Hertz and angular frequency ω_n in radians/seconds,

$$s_n \rightarrow \tau_n, \quad f_n = \frac{1}{\tau_n}.$$

Let $G = 2$ and allow the order N be non-integer but greater than zero.

$$\tau_n = \tau_0 2^{\frac{n}{N}}, \quad n \in \mathbb{Z}, \ N \in \mathbb{R} > 0$$

$$\omega_c = 2\pi$$

$$\omega_n = \frac{\omega_c}{\tau_n} = \frac{2\pi}{\tau_0}2^{-\frac{n}{N}} = \omega_0 2^{-\frac{n}{N}}.$$

The canonical unit-norm variation of the Gabor wavelet becomes

$$\Psi_{u,n}(t) = \frac{1}{\sqrt{\tau_n}}\Psi\left(\frac{t-u}{\tau_n}\right) = \frac{1}{[\pi(\sigma\tau_n)^2]^{1/4}}exp\left\{-\frac{1}{2}\left[\frac{t-u}{\sigma\tau_n}\right]^2\right\}exp\left\{i2\pi\left[\frac{t-u}{\tau_n}\right]\right\}$$

The Gabor-Morlet wavelet has apparent degrees of freedom that are not actually free when one standardizes to constant-Q band specifications. The next section locks down all the wavelet parameters..

Appendix C. The Quantum Wavelet

The Inferno framework was developed with the introduction of multiresolution array processing in the field of infrasound. Garces (2013) represented the time duration, or lifetime, of an analysis window at a specific period as

$$T_n = M_N\, \tau_n$$

This time window generally sets the temporal resolution of the resulting data products. On the case of the STFT, the analysis window can be referred to as the window of integration. In other words, the integration window T_n is defined as a multiple M_N of the pseudo period. This window immediately constrains the lowest frequency f_{min} that can be represented and the resolution of a spectral representation,

$$f_{min} = \frac{1}{T_n}$$

The upper bandwidth of the analysis window is set by the Nyquist frequency, which is half of the sampling frequency of the digital time series. In practice the upper bandwidth is close to one quarter of Nyquist. Although this representation is simple and tidy, it is not particularly informative. A more useful representation of how the window duration is the number of wavelet oscillations in the window, which can be represented by the quality factor Q_N of the wave function. As presented in Appendix D, the relation between the scale multiplier M_N and the quality factor can be estimated by the ½ power (-3dB) points on the power spectrum,

$$M_N = 2\sqrt{ln2}\; Q_N$$

$$\sigma = \frac{M_N}{2\pi} = \frac{\sqrt{ln2}}{\pi} Q_N$$

so that

$$\sigma\tau_n = \frac{M_N}{\omega_n} = \frac{T_n}{2\pi} = 2\sqrt{ln2}\frac{Q_N}{\omega_n}$$

The wavelet admissibility condition for the for this wavelet is equivalent to the zero mean, or

$$\sigma^2 \omega_c{}^2 = M_N^2 \gg 1$$

which is essentially met by the standard bands presented in Table 1. Although traditionally Nth octave frequencies are represented by the geometric mean of the band edge frequencies (Appendix A), in the evaluation of spectral power losses it is important to use the arithmetic mean for ω_n which would be centered in the bandwidth $\Delta\omega_n$ in linear frequency space. Since the ratios of the arithmetic and geometric means are constant and set by the band order N, the geometric scaling is still preserved.

The ratio of the Multiplier to the angular frequency is the scaled variance and recurs routinely in numerical evaluations. We define this term as the scaled lifetime $\widecheck{T}_n$ of a scale τ_n

$$\widecheck{T}_n = \frac{M_N}{\omega_n} = \frac{M_N}{2\pi}\tau_n = \frac{T_n}{2\pi}$$

Direct substitution yields the expressions for the wavelet transform pair,

$$\Psi_{u,n}(t) = \pi^{-\frac{1}{4}} \breve{T}_n^{-\frac{1}{2}} exp\left\{-\frac{1}{2}\left[\frac{t-u}{\breve{T}_n}\right]^2\right\} exp\{i\omega_n(t-u)\}$$

$$\widehat{\Psi}_{u,n}(\omega) = (4\pi)^{\frac{1}{4}} \breve{T}_n^{\frac{1}{2}} exp\left\{-\frac{1}{2}\left[\breve{T}_n(\omega-\omega_n)\right]^2\right\} exp\{-i\omega u\} .$$

and the peak-unit-spectrum variations used on more recent computational implementations (e.g. Mallat, 2012, 2019),

$$\psi_{u,n}(t) = (2\pi)^{-\frac{1}{2}} \breve{T}_n^{-1} exp\left\{-\frac{1}{2}\left[\frac{t-u}{\breve{T}_n}\right]^2\right\} exp\{i\omega_n(t-u)\}$$

$$\widehat{\psi}_{u,n}(\omega) = exp\left\{-\frac{1}{2}\left[\breve{T}_n(\omega-\omega_n)\right]^2\right\} exp\{-i\omega u\}$$

where

$$\Psi_{u,n}(t) = (4\pi)^{\frac{1}{4}} \breve{T}_n^{\frac{1}{2}} \psi_{u,n}(t), \qquad \breve{T}_n = \frac{M_N}{2\pi}\tau_n$$

It is important to recognize that, although the variables t, u can be interpreted as time and ω_n as the angular oscillation frequency of a sinusoid in radians, in digital signal processing these variables are dimensionless, as are the wavelets themselves. The typical scaling parameter for time is the digital sample rate in samples per second (referred to as Hz) or alternatively the sample interval, in seconds. The exact physical units are not important, although they reveal the implicit metrics of individuals and communities. Groups that work with long-lasting processes may use sample intervals in minutes, hours, or longer. Communities that focus on the frequency response of systems may prefer scaling by the angular frequency, or the Nyquist frequency.

Let f_s denote the sample rate in samples per seconds (Hz), with corresponding sample interval $\tau_s = 1/f_s$ in seconds/sample. Substitute all times for nondimensional parameters

$$t, \tau_n \longrightarrow x = f_s t, \ x_n = f_s \tau_n$$

that will have equivalent units of samples. The expression for the dimensionless scaled lifetime is

$$\breve{T}_n \longrightarrow \breve{X}_n = M_N \frac{f_s \tau_n}{2\pi}$$

and the angular frequency is modified

$$\omega_n \longrightarrow \bar{\omega}_n = \frac{2\pi f_n}{f_s} = \frac{2\pi}{f_s \tau_n} = \frac{M_N}{\breve{X}_n}$$

with corresponding nondimensional wavelet

$$\Psi_{x',n}(t) = \frac{1}{\pi^{1/4}}\frac{1}{\sqrt{\breve{X}_n}} exp\left\{-\frac{1}{2}\left[\frac{x-x'}{\breve{X}_n}\right]^2\right\} exp\left\{iM_N\left[\frac{x-x'}{\breve{X}_n}\right]\right\}$$

One can repeat this exercise on the second form

$$\psi_{x',n}(t) = (2\pi)^{-\frac{1}{2}} s_n^{-1} \, exp\left\{-\frac{1}{2}\left[\frac{x-x'}{s_n}\right]^2\right\} exp\left\{i2\pi \frac{f_n}{f_s}(x-x')\right\}$$

applying

$$s_n = s_0 \, 2^{\frac{n}{N}},$$

yields

$$\psi_{x',n}(t) = (\pi \, 2s_0^2)^{-\frac{1}{2}} [s_n]^{-1} \, exp\left\{-\frac{1}{2s_0^2}\left[\frac{x-x'}{s_n}\right]^2\right\} exp\left\{i\frac{M_N}{s_0}\left[\frac{x-x'}{s_n}\right]\right\}$$

which has the form

$$\psi(\mu) = \frac{1}{\sqrt{\pi b}} \, exp\left\{-\frac{\mu^2}{b}\right\} exp\{i\bar{\omega}_b \, \mu\}$$

$$\psi_{\mu',n}(t) = \frac{1}{s_n} \psi\left(\frac{\mu-\mu'}{s_n}\right)$$

with

$$s_n = 2^{\frac{n}{N}}, \ n \ge 0, \qquad s_0 = M_N \frac{f_s \tau_0}{2\pi}$$

$$b = 2s_0^2 = 2\left[M_N \frac{f_s \tau_0}{2\pi}\right]^2 = 2\left[\frac{M_N}{\bar{\omega}_b}\right]^2$$

$$\bar{\omega}_b = \frac{\omega_0}{f_s} = 2\pi \frac{f_0}{f_s} = \frac{2\pi}{f_s \tau_0}$$

Note that since

$$b = 2\left(\frac{M_N}{\bar{\omega}_0}\right)^2 = 2\left(2\sqrt{ln2}\frac{Q_N}{\bar{\omega}_0}\right)^2 = 8ln2\left(\frac{f_s}{\Delta\omega_0}\right)^2$$

the "bandwidth" b is inversely proportional to the actual bandwidth of the highest frequency.

In returning to the main text, the scale multiplier M_N will be renamed Ω_N to better match the canonical computational representation of the Gabor atoms.

Appendix D. The Q of Base 2

The natural base for both contemporary and quantum computers is base 2, and analysis windows with powers of two are recommended for complex computations at large scales. Many efficient algorithms are based on binary (base two) filter banks. Selecting $G = 2$ yields

$$\frac{S_C}{S_0} = 2^{\frac{n}{N}}, \qquad \frac{S_H}{S_C} = 2^{\frac{1}{2N}}, \qquad \frac{S_L}{S_C} = 2^{-\frac{1}{2N}}, \qquad \frac{S_H S_L}{S_C^2} = 1$$

Define the nth center scale s_n as a time scale τ_n,

$$\tau_n = S_C$$

Which, from eq. (), yields an angular frequency ω_n

$$\omega_n = \frac{2\pi}{\tau_n} = \frac{2\pi}{\tau_0} 2^{-\frac{n}{N}}$$

with

$$\frac{\Delta\omega_n}{\omega_n} = \frac{1}{Q_N} = \frac{1}{\sqrt{2}N}$$

Although the center frequency is traditionally defined as the geometric mean of the band edges, the ½ power spectral points at the band edges are only symmetric around the arithmetic mean of the center frequency. The relation between the arithmetic mean $\omega_{na} = (\omega_L + \omega_H)/2$ and the geometric mean $\omega_{ng} = \sqrt{\omega_L \omega_H}$ of the center frequency of fractional binary bands is

$$\frac{\omega_{na}}{\omega_{ng}} \cong \sqrt{1 + \frac{1}{8N^2}} \approx 1 + \frac{1}{16N^2}$$

where the approximation uses the binomial expansion. The arithmetic and geometric center frequencies are close to each other, and for fractional octave bands (N>1) get ever tighter. However, the band edge power levels at the half band width $\Delta\omega_n/2$ should be considered to be relative to the arithmetic mean rather than the geometric mean. In general practice it is easier to use the arithmetic frequency as ω_n, with the understanding that the fractional octave specifications are defined by geometric scaling.

The power spectral density of the Gabor wavelet is:

$$\widehat{\Psi}^2{}_{u,n}(\omega) = [4\pi]^{1/2}(\sigma\tau_n)\, exp\{-[\sigma\tau_n]^2[\omega - \omega_n]^2\}$$

$$\frac{\widehat{\Psi}^2{}_{u,n}(\omega_n \pm \Delta\omega_n/2)}{\widehat{\Psi}^2{}_{u,n}(\omega_n)} = exp\{-[\sigma\tau_n]^2[\Delta\omega_n/2]^2\} = exp\left\{-[\sigma\tau_n]^2\left[\frac{\omega_n}{2Q_N}\right]^2\right\} = \frac{1}{Y}$$

Where Y is the fractional power loss.

$$\left[\sigma\tau_n\frac{\omega_n}{2Q_N}\right]^2 = ln(Y)$$
$$[2\pi\sigma]^2 = Q_N^2\, 4ln(Y)$$

where to convert from a fractional power loss Y to X in decibels, one can use

$$X\, dB = 10\, log_{10}(Y)\,.$$

There exist various definitions of the quality factor of a system. This paper defines Q_N by the -3dB spectral power relative to the peak spectral power.

Defining the Multiplier as

$$M_G = M_N = 2\pi\sigma$$

where the Gabor window duration is

$$T_n = M_N\, \tau_n$$

and evaluating at the -3dB points for Y = 2, the product of the standard deviation and the scale of the Gaussian envelope can now be redefined as the wavelet scaled lifetime in cycles

$$\sigma\tau_n = \frac{M_N}{\omega_n} = \frac{T_n}{2\pi} = \frac{Q_N}{\omega_n} 2\sqrt{ln(2)}$$

$$M_N = 2\sqrt{ln(2)}\, Q_N$$

$$\sigma = \frac{\sqrt{ln2}}{\pi}\, Q_N \approx 0.265\, Q_N$$

Direct substitution yields

$$\Psi_{u,n}(t) = \frac{1}{\left[\pi\left(\frac{M_N}{\omega_n}\right)^2\right]^{1/4}} exp\left\{-\frac{1}{2}\left[\frac{\omega_n(t-u)}{M_N}\right]^2\right\} exp\{i\omega_n(t-u)\}$$

Although the unit norm variation of the Morlet-Gabor wavelet leads to some simplifications when computing the Gabor box in the next section, the alternate forms have the scaling

$$\psi_H(t) = \frac{1}{\tau_n}\, \psi_H\left(\frac{t-u}{\tau_n}\right)$$

with unit peak spectrum at $\omega = \omega_n$. Applying the expressions developed above and the preferred scaling yields

$$\psi_H(t) = \frac{1}{\sqrt{2\pi}}\frac{\omega_n}{M_N}\, exp\left\{-\frac{1}{2}\left[\frac{\omega_n(t-u)}{M_N}\right]^2\right\} exp\{i\omega_n(t-u)\}$$

$$\hat{\psi}_H(\omega) = exp\left\{-\frac{1}{2}\left[\frac{M_N}{\omega_n}(\omega-\omega_n)\right]^2\right\} exp\{-i\omega u\}$$

The resulting units on the wave function are 1/seconds, and the Fourier transform is dimensionless.

Consider

$$\left|\hat{\psi}_H\left(\omega + \delta\frac{\Delta\omega_n}{2}\right)\right|^2 = exp\left\{-\left[\frac{M_N}{\omega_n}\left(\delta\frac{\Delta\omega_n}{2}\right)\right]^2\right\} = exp\left\{-\left[\delta\sqrt{ln(2)}\right]^2\right\} = 2^{-\delta^2}$$

where

$$\frac{M_N}{2Q_N} = \sqrt{ln(2)}$$

$$dB = 10*log_{10}(2^{-\delta^2}) = -\delta^2 10*log_{10}(2) \approx -3\delta^2$$
$$bR = \frac{1}{2}log_2(2^{-\delta^2}) = \frac{-\delta^2}{2}$$

so there is a loss of 3dB, 12dB, 27dB, and 48dB, and a binary power loss of ½, 2, 4.5, and 8 fbits, for integer multiples of the bandedge $\delta = 1, 2, 3, 4$, respectively.

It is worth considering an alternate definition for the quality factor of an oscillator. Consider the time required for the amplitude to drop to 1/e of its peak value. In the case of the Quantum wavelet this is set by the Gaussian envelope, and this particular definition is best suited for the real part of the wavelet which is symmetric about the origin. By applying this definition,

$$exp\left\{-\frac{1}{2}\left[\frac{\omega_n\tau_e}{M_N}\right]^2\right\} = exp\{-1\}$$

$$\tau_e = \frac{\sqrt{2}}{\pi}\frac{T_n}{2} \approx 0.45\frac{T_n}{2}$$

Since the wavelet is symmetric, this states that the portion of the wavelet contained within $2\tau_e$ of the window has an amplitude above 1/e of the peak. The quality factor associated with this type of oscillator is

$$Q_e = \frac{\omega_n \tau_e}{2} = \frac{M_N}{\sqrt{2}}$$

and comparison with the -3dB quality factor shows

$$Q_e = \sqrt{2ln(2)}\ Q_N \approx 1.1774\ Q_N$$

and they are sufficiently close to each other to be equivalent for descriptive purposes. The time support of the quantum wavelet is defined by

$$T_n = M_N\ \tau_n = 2\sqrt{ln(2)}\ Q_N \tau_n$$

where $Q_N \approx Q_e$ can be interpreted as the number of oscillations in a little less than half of the total window T_n with amplitude above 1/e of the maximum amplitude. The remaining half of the window is useful to allow the wavelet to settle down and meet the desirable condition of a vanishing first moment.

Practical implementations of Gabor wavelets and their variants often have to make some compromises in the application of the wavelet duration T_n, in particular if the window is required to be a power of two. Direct integration of the wavelet power over the window T_n shows that it contains 99.999% of all the power. Integration over $2\tau_e$ will be insufficient. However, there exists a third quality factor defined by

$$exp\left\{-\frac{1}{2}\left[\frac{\omega_n \tau_\pi}{M_N}\right]^2\right\} = exp\{-\pi\}$$

where

$$Q_\pi = \frac{\omega_n \tau_\pi}{2}$$
$$Q_\pi = \sqrt{\pi}\ Q_e \approx 1.7724\ Q_e$$

$$\tau_\pi = \sqrt{\pi}\ \tau_e = \sqrt{\frac{2}{\pi}}\frac{T_n}{2} \approx 0.7978\frac{T_n}{2}$$

In other words, $2\tau_\pi$ encompasses ~80% of the window, and integration of the wavelet power over $2\tau_\pi$ returns 99.96% of the total power. Therefore $2\tau_\pi = 0.8T_n$ may be a reasonable lower bound for the wavelet duration. This is further considered in the next Appendix.

Appendix E. The Gabor Box

Gabor introduced the time-frequency uncertainty principle in his landmark 1946 paper. It is not possible to observe for all time and reach zero frequency. It is also impossible to sample infinitely fast and reach infinite frequency. All observations require a restriction in the observation time and the observation rate, and this places hard limits on the observable bandwidth of a process. The fundamental discretization interval scale invokes the Gabor uncertainty principle, which states the time and period of

a signal cannot be known exactly but can be contained inside the box defined by the temporal and frequency variance of the probability distribution of the wave function.

This section follows the generalized mathematical formalism of M9, Section 2.3.2, Uncertainty Principle. As in M9 and Garces (2019), the Fourier Transform pair used in this work is

$$\hat{f}(\omega) = \int_{-\infty}^{\infty} f(t)e^{-j\omega t}\, dt$$

$$f(t) = \frac{1}{2\pi}\int_{-\infty}^{\infty} \hat{f}(\omega)e^{j\omega t}\, d\omega \ ,$$

where $\hat{f}(\omega)$ and $f(t)$ may be complex.

The Parseval-Plancherel identity asserts that

$$\|f\|^2 = \int_{-\infty}^{\infty} |f(t)|^2\, dt = \frac{1}{2\pi}\int_{-\infty}^{\infty} \left|\hat{f}(\omega)\right|^2 d\omega = \frac{1}{2\pi}\|\hat{f}\|^2$$

where

$$|f|^2 = f \cdot f^*$$

and the asterix denotes complex conjugation. A related identity the for product is routinely used in Fourier and Wavelet analyses and the application of filter banks.

$$\int_{-\infty}^{\infty} f(t)g^*(t)\, dt = \frac{1}{2\pi}\int_{-\infty}^{\infty} \hat{f}(\omega)\hat{g}^*(\omega)\, d\omega$$

The Gabor uncertainty principle constrains uncertainty to Gabor box defined by the variance in time and frequency. It is equivalent to the Heisenberg uncertainty principle for position and momentum extended to time and frequency, or space and wavenumber. Let a one-dimensional signal of interest be represented by a wave function $f(t)$. The probability density that a signal can be localized in time at a given time t is

$$\frac{|f(t)|^2}{\|f\|^2} = \frac{2\pi|f(t)|^2}{\|\hat{f}\|^2},$$

and the probability density that its angular frequency is ω is

$$\frac{|\hat{f}(\omega)|^2}{\|\hat{f}\|^2} = \frac{|\hat{f}(\omega)|^2}{2\pi\|f\|^2}.$$

The average time (center) of the signal can be expressed as

$$u = \frac{1}{\|f\|^2}\int_{-\infty}^{\infty} t\, |f(t)|^2\, dt$$

and the variance in the time localization of the signal as

$$\sigma_t^2 = \frac{1}{\|f\|^2}\int_{-\infty}^{\infty} (t-u)^2\, |f(t)|^2\, dt.$$

The average, or central frequency, of the spectrum can be expressed as

$$\xi = \frac{1}{\|\hat{f}\|^2} \int_{-\infty}^{\infty} \omega \, |\hat{f}(\omega)|^2 \, d\omega$$

and the variance in the frequency localization of the signal as

$$\sigma_\omega^2 = \frac{1}{\|\hat{f}\|^2} \int_{-\infty}^{\infty} (\omega - \xi)^2 \, |\hat{f}(\omega)|^2 \, d\omega.$$

M9 uses these expressions to rederive the Heisenberg-Gabor uncertainty principle, which states that the temporal and angular frequency variance satisfy:

$$\sigma_t^2 \sigma_\omega^2 \geq \frac{1}{4}$$

In the special case of the Gabor-Morlet wavelet and its Quantum spawn, where the wave function is symmetric and centered around the time-shift u and the spectrum is symmetric relative to the peak frequency ω_n, the variance for the time and frequency distribution of the signal wave function can be readily evaluated.

$$\psi_H(t) = \frac{1}{\sqrt{2\pi}} \frac{\omega_n}{M_N} \exp\left\{-\frac{1}{2}\left[\frac{\omega_n(t-u)}{M_N}\right]^2\right\} \exp\{i\omega_n(t-u)\} = \frac{1}{\sqrt{2\pi}} \frac{1}{\breve{T}_n} \exp\left\{-\frac{1}{2}\left[\frac{t-u}{\breve{T}_n}\right]^2\right\} \exp\{i\omega_n(t-u)\}$$

$$\hat{\psi}_H(\omega) = \exp\left\{-\frac{1}{2}\left[M_N\left(\frac{\omega}{\omega_n}-1\right)\right]^2\right\} \exp\{-i\omega u\} = \exp\left\{-\frac{1}{2}[\breve{T}_n(\omega-\omega_n)]^2\right\} \exp\{-i\omega u\}$$

$$|\psi_H(t)|^2 = \frac{1}{2\pi}\left(\frac{\omega_n}{M_N}\right)^2 \exp\left\{-\left[\frac{\omega_n(t-u)}{M_N}\right]^2\right\} = \frac{1}{2\pi}\breve{T}_n^{-2} \exp\left\{-\left[\frac{t-u}{\breve{T}_n}\right]^2\right\}$$

$$|\hat{\psi}_H(\omega)|^2 = \exp\left\{-\left[M_N\left(\frac{\omega}{\omega_n}-1\right)\right]^2\right\} = \exp\left\{-[\breve{T}_n(\omega-\omega_n)]^2\right\}$$

$$\|\psi_H\|^2 = \frac{\sqrt{\pi}}{2\pi}\left(\frac{\omega_n}{M_N}\right) = \frac{\sqrt{\pi}}{2\pi}\breve{T}_n^{-1}$$

$$\|\hat{\psi}_H\|^2 = \sqrt{\pi}\left(\frac{\omega_n}{M_N}\right) = \sqrt{\pi}\,\breve{T}_n^{-1}$$

$$\frac{1}{\|\psi_H\|^2} \int_{-\infty}^{\infty} (t-u) \, |\psi_H(t-u)|^2 \, dt = 0$$

$$\frac{1}{\|\hat{\psi}_H\|^2} \int_{-\infty}^{\infty} (\omega-\omega_n) \, |\hat{\psi}_H(\omega-\omega_n)|^2 \, d\omega = 0$$

$$\sigma_t^2 = \frac{1}{\|\psi_H\|^2} \int_{-\infty}^{\infty} (t-u)^2 \, |\psi_H(t-u)|^2 \, dt = \frac{1}{2}\breve{T}_n^2$$

$$\sigma_{\omega n}^2 = \frac{1}{\|\hat{\psi}_H\|^2} \int_{-\infty}^{\infty} (\omega-\omega_n)^2 \, |\hat{\psi}_H(\omega-\omega_n)|^2 \, d\omega = \frac{1}{2}\breve{T}_n^{-2}$$

and the Gabor box defined by the variance is minimal,

$$\sigma_t^2 \sigma_{\omega n}^2 = \frac{1}{4},$$

which is another reason for this wavelet's popularity.

Consider the standard deviation for time integrated over the scaled window $\epsilon 2\pi \breve{T}_n = \epsilon T_n$

$$\sigma_t^2(\epsilon) = \frac{1}{\|\psi_H\|^2} \int_{u-\frac{\epsilon T_n}{2}}^{u+\frac{\epsilon T_n}{2}} (t-u)^2 \, |\psi_H(t-u)|^2 \, dt = \frac{1}{\sqrt{\pi}} \left[\frac{M_N}{\omega_n}\right]^2 \int_{-\epsilon\pi}^{\epsilon\pi} x^2 \, e^{-x^2} \, dx$$

$$\int_{-a}^{a} x^2 \, e^{-x^2} \, dx = \frac{\sqrt{\pi}}{2} \left[erf(a) - \frac{2}{\sqrt{\pi}} a \, e^{-a^2}\right]$$

For $\epsilon \geq \frac{3}{2\pi}$

$$\sigma_t^2(\epsilon) \cong \frac{1}{2} \breve{T}_n^2 \, erf(\epsilon\pi)$$

For $\epsilon = [1.0, 0.8, 0.45]$

$$\sigma_t^2(\epsilon) \cong \frac{1}{2} \breve{T}_n^2 \, [0.9999, 0.9996, 0.9544]$$

where ϵ corresponds to integration over T_n, $2\tau_\pi \approx 0.8 T_n$, and $2\tau_e \approx 0.45 T_n$, corresponding to the full window, the decay time associated with Q_π, and the e-folding time associated with Q_e, respectively (Appendix D).

Next, consider the standard deviation for time integrated over the scaled window ϵT_n

$$\sigma_{\omega_n}^2(\delta) = \frac{1}{\|\hat{\psi}_H\|^2} \int_{\omega_n-\frac{\delta\Delta\omega_n}{2}}^{\omega_n+\frac{\delta\Delta\omega_n}{2}} (\omega-\omega_n)^2 \, \left|\hat{\psi}_H(\omega-\omega_n)\right|^2 \, d\omega = = \frac{1}{\sqrt{\pi}} \left[\frac{M_N}{\omega_n}\right]^{-2} \int_{-\delta\sqrt{ln2}}^{\delta\sqrt{ln2}} x^2 \, e^{-x^2} \, dx$$

$$\sigma_{\omega_n}^2(\delta) \cong \frac{1}{2} \breve{T}_n^{-2} \left[erf(\delta\sqrt{ln2}) - \frac{2}{\sqrt{\pi}}(\delta\sqrt{ln2}) \, 2^{-\delta^2}\right]$$

For $\delta = [1, \ 2, \ 3, \ 4]$

$$\sigma_{\omega_n}^2(\delta) \cong \frac{1}{2} \breve{T}_n^{-2} \, [0.2912, 0.8640, 0.9941, 0.9999]$$

where δ corresponds to integration over $\Delta\omega_n, 2\Delta\omega_n, 3\Delta\omega_n, and \ 4\Delta\omega_n$, respectively. These results show that the Gabor box can be well approximated (>99% of the variance) by a window of duration $2\tau_\pi = 0.8 T_n$ and a bandwidth of $3\Delta\omega_n$, and over 99.99% of the variance is contained by a Gabor box of dimensions $T_n, 4\Delta\omega_n$. In other words, third octave bands will contain over 99% of the variance within its octave and within 80% of the full window T_n.

Appendix F. The Gabor Family

A few variations of the Gabor-Morlet wavelet are available in present-day computing environments.

One of the more familiar forms of the mother wavelet is

$$\psi(\mu) = \frac{1}{\sqrt{\pi b}} \, exp\left\{-\frac{\mu^2}{b}\right\} exp\{i2\pi \bar{f}_b \, \mu\}$$

$$\psi_{\mu',n}(t) = \frac{1}{s_n} \psi\left(\frac{\mu - \mu'}{s_n}\right)$$

This form is found in the Matlab "cmor" function as well as the Python Pywavelets "cmorB-C" function with $C = \bar{f}_b$. The term b is referred to as the "bandwidth parameter" of the wavelet. The Quantum wavelet has the equivalence

$$s_n = 2^{\frac{n}{N}}, \ \ n \geq 0,$$

$$\tau_n = \tau_0 s_n = \frac{1}{f_0} s_n$$

$$b = 2\left[M_N \frac{f_s \tau_0}{2\pi}\right]^2$$

$$C = \bar{f}_b = \frac{f_0}{f_s} = \frac{1}{f_s \tau_0}$$

Where f_0, the highest center frequency, is used as the starting point. The scaled wavelet duration is $M_N \frac{f_s}{f_n}$ and can be rounded to approximate the number of points for each scale.

Foster (1996) expresses the abbreviated Morlet wavelet as

$$F(z) = e^{iz - cz^2} = exp\left\{i\omega_n t - \frac{1}{2M_N^2}\omega_n^2 t^2\right\}$$

So that $z = \omega_n t$ and now $c = \frac{1}{2M_N^2}$ is inversely proportional to the Q of the wave function. The beauty of Foster's approach is that it can be used for unevenly sampled data. A similar functional representation is also used in the Scipy function scipy.signal.gausspulse, which is expressed as:

$$G(t) = e^{i\omega_n t - at^2} = exp\left\{i2\pi f_n t - \left[\frac{\omega_n^2}{2M_N^2}\right]t^2\right\}$$

For the quantum wavelet, the -3dB reference level specification (gausspole bwr) yields the fractional bandwidth

$$bwr = \frac{\Delta\omega_n}{\omega_n} = \frac{1}{Q_N}$$

and used as input. Note the default reference level for scipy.gausspulse is *bwr* = -6dB and it should be overridden to -3dB to reproduce the quantum wavelet. The scaling equivalence is

$$\psi_H(t) = \frac{1}{\sqrt{2\pi}} \breve{T}_n^{-1} \, G(t) = \frac{\sqrt{2\pi} f_n}{M_N} G(t)$$

Appendix G. The Analytic Function for the GT Blast Pulse

The reconstruction coefficients of the complex Morlet CWT return the imaginary part of the analytic signal. The complex analytic signal corresponding to the real signal $g(\hat{t})$ is

$$g_{\mathbb{C}}(\hat{t}) = g(\hat{t}) + j \, \mathcal{H}[g(\hat{t})]$$

Where $\mathcal{H}$ denotes the Hilbert transform, a recurrent topic in wave propagation as reflection introduces phase shifts that are often modeled as Hilbert transforms of the original signal (e.g. Brekhovski, 1980). For example, some of the U-shaped infrasound waveforms associated with thermospheric returns resemble the Hilbert transform of an explosion pulse (e.g. Vergoz et al. 2019). The Hilbert transform is also useful for estimating instantaneous frequency and in the computation of the Hilbert-Huang transform (e.g. Huang and Wu, 2008).

Let $g(\hat{t})$ represent the GT pulse,

$$g(\hat{t}) = (1 - \hat{t}), \quad 0 \le \hat{t} \le 1$$

$$g(\hat{t}) = \frac{1}{6}(1 - \hat{t})(1 + \sqrt{6} - \hat{t})^2, \quad 1 < \hat{t} \le 1 + \sqrt{6} \ .$$

The Hilbert transform of the canonical GT blast pulse is rather unwieldy, but can be evaluated from

$$g_{\mathcal{H}}(\hat{t}) = \mathcal{H}[g(\hat{t})] = \mathcal{P}\frac{1}{\pi}\int_{-\infty}^{\infty}\frac{g(x)}{t - x}dx$$

Where the $\mathcal{P}$ in front of the integral denotes the Chaucy principal value. Multiple integration by parts over the interval of the GT pulse yields

$$g_{\mathcal{H}}(\hat{t}) = \frac{1}{\pi}[1 + (1 - \hat{t})ln(-\hat{t}) - (1 - \hat{t})ln(1 - \hat{t})], \qquad 0 \le \tau \le 1$$

$$g_{\mathcal{H}}(\hat{t}) = \frac{1}{6\pi}\frac{(a - 1)}{6}[a(2a + 5) - 1 + 6\hat{t}^2 - 3\hat{t}(1 + 3a)]$$

$$+ \frac{1}{6\pi}[(\hat{t} - 1)(a - \hat{t})^2][ln(a - \hat{t}) - ln(1 - \hat{t})], \quad 1 < \tau \le a = 1 + \sqrt{6}.$$

Since

$$\lim_{x \to 0} x \, ln(x) = 0, \qquad \lim_{x \to 0} x^2 \, ln(x) = 0$$

The solutions are well behaved near the zero crossings. However, there are some issues in this solution. First, there are the two troublesome implicitly complex terms. The first is

$$ln(-\hat{t}) = ln(\hat{t}) + j\pi, \qquad 0 \le \tau \le 1$$

where $ln(\hat{t})$ tends to negative infinity at $\hat{t} = 0$. The second tricky term is

$$ln(1 - \hat{t}) = ln(\hat{t} - 1) + j\pi, \qquad 1 < \tau \le 1 + \sqrt{6}$$

The complex terms are awkward; fortunately, multiplication and division by zero can be readily avoided numerically by adding the smallest floating point value (float epsilon) to arguments in logarithmic computations so it is possible to evaluate the real part of the solution. Another inconvenience is the discontinuity in $g_{\mathcal{H}}$ and its slope as $\hat{t} \to 1$. Rewriting the first term as

$$g_{\mathcal{H}}(\hat{t})_{\hat{t}<1} = \frac{1}{\pi}[1 + (1 - \hat{t})ln(\hat{t}) - (1 - \hat{t})ln(1 - \hat{t})] + j(1 - \hat{t}), \qquad \hat{t} \to 1 \, from \, below$$

$$g_{\mathcal{H}}(\hat{t} \to 1) = \frac{1}{\pi}$$

Evaluating the second term yields

$$g_{\mathcal{H}}(\hat{\tau} = 1) = \frac{1}{\pi}\frac{\sqrt{2}}{\sqrt{3}} = \frac{1}{\pi}\left[1 - \frac{\sqrt{3} - \sqrt{2}}{\sqrt{3}}\right], \qquad \hat{\tau} \to 1 \; from \; above$$

These deficiencies are suboptimal, and not altogether surprising given that Garces (2019) did not design integrability into the GT pulse. Fortunately, these inadequacies are deemed computationally irrelevant by using the numerical convolution provided by the SciPy signal.hilbert, which returns the analytic function for an input real signal. The comparison between the unfiltered synthetic theoretical analytic signals, the CWT reconstruction, and the numerical Hilbert transform are presented in the figures in the main text.

Funding: This material is based upon work supported in part by the Department of Energy National Nuclear Security Administration under Award Numbers DE-XXXX and the Air Force Research Laboratory under agreement FAXXXX.

Disclaimer: This report was prepared as an account of work sponsored by an agency of the United States Government. Neither the United States Government nor any agency thereof, nor any of their employees, makes any warranty, express or implied, or assumes any legal liability or responsibility for the accuracy, completeness, or usefulness of any information, apparatus, product, or process disclosed, or represents that its use would not infringe privately owned rights. Reference herein to any specific commercial product, process, or service by trade name, trademark, manufacturer, or otherwise does not necessarily constitute or imply its endorsement, recommendation, or favoring by the United States Government or any agency thereof. The views and opinions of authors expressed herein do not necessarily state or reflect those of the United States Government or any agency thereof.

Acknowledgments: This is where I thank the reviewers, official or unofficial.

Conflicts of Interest: The author declares no conflict of interest. The funders had no role in the design of the study; in the collection, analyses, or interpretation of data; in the writing of the manuscript, or in the decision to publish the results.

References

1. Garcés, M. A. (2013). On infrasound standards, Part 1. Time, frequency, and energy scaling. Inframatics, 2, 13-35, doi:10.4236/inframatics.2013.22002.
2. Gabor, D., Theory of Communication, Part 3, Electrical Engineers, Vol. 93, No. 26, 1946, pp. 445-457.
3. Pacenak, Z., Kleissl, J., and E. Lam, "Detection of a Surface Detonated Nuclear Weapon using a Photovoltaic Rich Microgrid", IEEE Power and Energy Society General Meeting, San Diego, CA, 1 Aug 2018.
4. Cai, Y., Lam, E., Howlett, T. Cai, A., "Spatiotemporal Analysis of 'Jello Effect' in Drone Videos", 10th International Conference on Applied Human Factors and Ergonomics, Washington D.C., USA, 26 July 2019.
5. Shannon, C. E., *The Mathematical Theory of Communication*. Urbana, IL, University of Illinois Press, 1998 [1949].
6. Ashmead,J. (2012). Morlet Wavelets in Quantum Mechanics. Quanta, 1(1), 58-70. doi:https://doi.org/10.12743/quanta.v1i1.5
7. Sheu, Yae-lin, Hsu, Liang-Yan, Wu, Hau-tieng, Li, Peng-Cheng, Chu, Shih-I, A new time-frequency method to reveal quantum dynamics of atomic hydrogen in intense laser pulses: Synchrosqueezing transform, AIP Advances 4, 117138 (2014); https://doi.org/10.1063/1.4903164
8. Canolty, Ryan T. and T. Womelsdorf, Multiscale Adaptive Gabor Expansion (MAGE): Improved Detection of Transient Oscillatory Burst Amplitude and Phase, 2019, bioRxiv 369116; doi: https://doi.org/10.1101/369116
9. Yu Shi and Xian-Da Zhang, "A Gabor atom network for signal classification with application in radar target recognition," in IEEE Transactions on Signal Processing, vol. 49, no. 12, pp. 2994-3004, Dec. 2001, doi: 10.1109/78.969508.
10. Grossmann, A. and J. Morlet, Decomposition of Hardy functions into square integrable wavelets of constant shape, Soc. Int. Am. Math. (SIAM), J. Math. Analys., Vol. 15, 1984, pp. 723-736.

11. Goupillaud, P., A. Grossmann, J. Morlet, Cycle-octave and related transforms in seismic signal analysis, Geoexploration, Vol 23, Issue 1, 1984, Pages 85-102, ISSN 0016-7142, https://doi.org/10.1016/0016-7142(84)90025-5.

12. Berg, N. J. and J. M. Pellegrino, Acousto-optic signal processing: theory and implementation, Marcel Dekker, NY, 1996, ISBN 0-8247-8925-3.

13. Li, T, and Zhou, M, ECG classification using wavelet packet entropy and random forests, Entropy 2016, 18, 285; doi:10.3390/e18080285.

14. Foster, G., Wavelets for period analysis of unevenly sampled time series, Astronomical J., Vol. 112(4), 1996, pp.1709-1729.

15. Mallat, S., A wavelet tour of signal processing: the sparse way, Academic Press, 1998, 3rd edn. 2009.

16. Mallat, S., Group invariant scattering. Comm. Pure Appl. Math., 65(10):1331–1398, 2012.

17. Mallat, S., Zhang, S., and Rochette, G., Phase Harmonic Correlations and Convolutional Neural Networks, IMA J. of Information and Inference, 2019.

18. Torrence, C., and G. P. Compo, 1998: A Practical Guide to Wavelet Analysis. Bull. Amer. Meteor. Soc., 79, 61–78, https://doi.org/10.1175/1520-0477(1998)079<0061:APGTWA>2.0.CO;2.

19. Farge, M., Wavelet transforms and their applications to turbulence, Annual Review of Fluid Mechanics, 1992 24:1, 395-458, doi: 10.1146/annurev.fl.24.010192.002143.

20. Lebedeva EA, Postnikov EB. On alternative wavelet reconstruction formula: a case study of approximate wavelets. R Soc Open Sci. 2014;1(2):140124. Published 2014 Oct 8. doi:10.1098/rsos.140124

21. Bishop, M., http://mark-bishop.net/signals/CWTReconstructionFactors.pdf, Last modified 2018-07-29.

22. Gregory R. Lee, Ralf Gommers, Filip Wasilewski, Kai Wohlfahrt, Aaron O'Leary (2019). PyWavelets: A Python package for wavelet analysis. Journal of Open Source Software, 4(36), 1237, https://doi.org/10.21105/joss.01237.

23. Pauli Virtanen, Ralf Gommers, Travis E. Oliphant, Matt Haberland, Tyler Reddy, David Cournapeau, Evgeni Burovski, Pearu Peterson, Warren Weckesser, Jonathan Bright, Stéfan J. van der Walt, Matthew Brett, Joshua Wilson, K. Jarrod Millman, Nikolay Mayorov, Andrew R. J. Nelson, Eric Jones, Robert Kern, Eric Larson, CJ Carey, İlhan Polat, Yu Feng, Eric W. Moore, Jake VanderPlas, Denis Laxalde, Josef Perktold, Robert Cimrman, Ian Henriksen, E.A. Quintero, Charles R Harris, Anne M. Archibald, Antônio H. Ribeiro, Fabian Pedregosa, Paul van Mulbregt, and SciPy 1.0 Contributors. (2020) SciPy 1.0: Fundamental Algorithms for Scientific Computing in Python. Nature Methods, in press.

24. Brekhovskikh, L., Waves in Layered Media, Second Edition, Elsevier, Oxford, 1980.

25. Garcés, M. A. (2019). Explosion Source Models, Chapter in Infrasound Monitoring for Atmospheric Studies, Second Edition, Springer, Switzerland, DOI 10.1007/978-3-319-75140_5, p. 273-345.

26. Vergoz, J., A. LePichon, and C. Millet (2019). The Antares explosion observed by the USArray: an unprecedented collection of infrasound phases recorded from the same event, Chapter in Infrasound Monitoring for Atmospheric Studies, Second Edition, Springer, Switzerland, DOI 10.1007/978-3-319-75140_5, p. 349-386.

27. Mialle, P. D. Brown, and N. Arora. (2019). Advances in operational processing at the international data center, Chapter in Infrasound Monitoring for Atmospheric Studies, Second Edition, Springer, Switzerland, DOI 10.1007/978-3-319-75140_5, p. 273-345.

28. Huang, N. E. and Z. Wu (2008). A review on Hilbert-Huang transform: method and its applications to geophysical studies. Reviews of Geophys., 46, GR2006/2008